NASA TECHNICAL NOTE

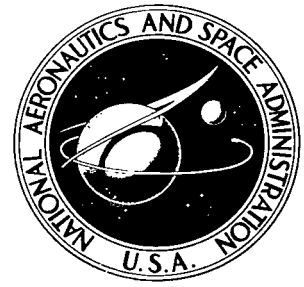

NASA TN D-6121

MINIMUM-MASS ISOTROPIC SHELLS OF REVOLUTION SUBJECTED TO UNIFORM PRESSURE AND AXIAL LOAD

by W. Jefferson Stroud

Langley Research Center
Hampton, Va. 23365

NATIONAL AERONAUTICS AND SPACE ADMINISTRATION • WASHINGTON, D. C. • FEBRUARY 1971

1. Report No.	2. Government Accession No.	3. Recipient's Catalog No.
NASA TN D-6121		

4. Title and Subtitle
MINIMUM-MASS ISOTROPIC SHELLS OF REVOLUTION SUBJECTED TO UNIFORM PRESSURE AND AXIAL LOAD

5. Report Date: February 1971

6. Performing Organization Code:

7. Author(s)
W. Jefferson Stroud

8. Performing Organization Report No.: L-5981

9. Performing Organization Name and Address
NASA Langley Research Center
Hampton, Va. 23365

10. Work Unit No.: 124-08-15-02

11. Contract or Grant No.:

12. Sponsoring Agency Name and Address
National Aeronautics and Space Administration
Washington, D.C. 20546

13. Type of Report and Period Covered: Technical Note

14. Sponsoring Agency Code:

15. Supplementary Notes: Part of the information presented herein was included in a thesis entitled "The Use of a Ritz Procedure in Determining Minimum Weight Shells of Revolution," submitted in partial fulfillment of the requirements for the degree of Doctor of Philosophy in Engineering Mechanics, Virginia Polytechnic Institute, Blacksburg, Virginia, June 1967.

16. Abstract

A method is presented for calculating the shape and thickness distribution of a minimum-mass shell of revolution for given coordinate and slope end conditions and given values of axial load and pressure load. The method makes use of linear membrane theory to relate the loading and shape to stress resultants and uses the strain energy of distortion (Von Mises) yield condition to relate the stress resultants to the thickness. The mass can then be expressed as an integral which is a function of shape. The integral is minimized by a Ritz procedure together with mathematical programing methods – that is, the shell shape is written in the form of a series of functions with undetermined coefficients, and the mass is minimized with respect to these coefficients. The shape, thickness distribution, and stress distributions are given for several examples.

17. Key Words (Suggested by Author(s))	18. Distribution Statement
Minimum-weight shells Nonlinear programing Mathematical programing	Unclassified – Unlimited

19. Security Classif. (of this report)	20. Security Classif. (of this page)	21. No. of Pages	22. Price*
Unclassified	Unclassified	43	$3.00

*For sale by the National Technical Information Service, Springfield, Virginia 22151

MINIMUM-MASS ISOTROPIC SHELLS OF REVOLUTION SUBJECTED TO UNIFORM PRESSURE AND AXIAL LOAD*

By W. Jefferson Stroud
Langley Research Center

SUMMARY

A method is presented for calculating the shape and thickness distribution of a minimum-mass shell of revolution for given coordinate and slope end conditions and given values of axial load and pressure load. The method makes use of linear membrane theory to relate the loading and shape to stress resultants and uses the strain energy of distortion (Von Mises) yield condition to relate the stress resultants to the thickness. The mass can then be expressed as an integral which is a function of shape. The integral is minimized by a Ritz procedure together with mathematical programing methods – that is, the shell shape is written in the form of a series of functions with undetermined coefficients, and the mass is minimized with respect to these coefficients. The shape, thickness distribution, and stress distributions are given for several examples.

INTRODUCTION

In the design of aerospace structures, it is important to keep the structural mass low while providing adequate structural integrity. Efforts to develop low-mass, high-strength aerospace structures have produced many efficient structural concepts, including stiffened-skin construction, sandwich construction, and composite materials. For certain structural applications the unstiffened isotropic shell of revolution is efficient. The present report examines unstiffened isotropic shells of revolution designed for minimum mass by adjusting both the shell shape and the thickness distribution. The loading is assumed to be a combination of axial load and uniform hydrostatic pressure.

Studies of low-mass isotropic shells of revolution have been performed from various viewpoints. The shell middle surface has been assumed to be defined and optimum thickness distributions of the shell wall for minimum mass have been determined in references 1 to 9. The shell wall thickness has been assumed constant and the optimum middle-surface shape has been determined in references 10 and 11. Finally, minimum-mass shells for which the wall thickness and middle-surface shapes are optimized

*Part of the information presented herein was included in a thesis entitled "The Use of a Ritz Procedure in Determining Minimum Weight Shells of Revolution," submitted in partial fulfillment of the requirements for the degree of Doctor of Philosophy in Engineering Mechanics, Virginia Polytechnic Institute, Blacksburg, Virginia, June 1967.

concurrently are considered in references 12 to 14. In all this previous work the failure criterion is assumed to be material yielding; buckling or wrinkling of the shell wall is not taken into consideration. Furthermore, except in reference 11, the shell middle-surface shapes are limited to very specific classes such as ellipsoidal or cylindrical, or to shapes characterized by only one or two shape parameters. Reference 11 considers shells which are closed at one end but which have a general middle-surface shape.

The object of the present report is to give a technique for calculating both the shape and the wall thickness distribution of a minimum-mass isotropic shell of revolution for given allowable geometric end conditions and given values of axial load and pressure load. This work is related, therefore, to that in references 12 to 14; however, the present work allows very general middle-surface shapes rather than being restricted to specific classes of shapes. In the present report, as in the previous work, the failure criterion is assumed to be yielding of the material, and buckling of the shell wall is not considered. Strictly speaking, since buckling is not considered, the present work is limited to thin-walled shells which are in tension at every point in the middle surface. In addition, variations in enclosed volume are not considered in the derivation of the minimum-mass configurations. In many cases, inequality constraints can be imposed during the synthesis process so that the resulting design will have no compressive stresses and/or so that the resulting design will enclose at least a minimum volume. Designs with inequality constraints on the stresses are considered in this report, but constraints on volume are not considered.

Linear membrane theory is used to derive all shapes and thickness distributions. Results for several examples are presented by means of nondimensional curves and tables.

SYMBOLS

The physical quantities in this paper are given both in the U.S. Customary Units and in the International System of Units (SI). Factors relating the two systems are given in reference 15; those factors used in the present paper are given in the appendix.

a_1, a_2, a_3 constants in expression for shell shape which are used to satisfy the boundary conditions (see eq. (32))

b depth of pressure-vessel head

$\bar{b}$ dimensionless depth of pressure-vessel head, b/y_o

$c_0, c_1, c_2, \ldots$ constants in expression for shell shape which are used to minimize the mass (see eqs. (31), (32), and (33))

F_o axial load per unit circumferential length applied to the shell at $x = 0$, positive when tensile

m mass of shell

$\bar{m}$ dimensionless mass, $m\sigma_c/\pi\rho p y_o^3$

N_θ, N_ϕ stress resultants in circumferential and meridional directions, respectively

$\bar{N}_\theta$ dimensionless circumferential stress resultant, $2N_\theta/py_o$

$\bar{N}_\phi$ dimensionless meridional stress resultant, $2N_\phi/py_o$

p pressure, positive when internal

R_1, R_2 shell radii of curvature (see eqs. (10) and (11))

s distance along meridian

$\bar{s}$ dimensionless distance along meridian, s/y_o

t thickness of shell wall

$\bar{t}$ dimensionless thickness, $2t\sigma_c/py_o$

x coordinate along shell axis of rotation, with origin at left end of shell

x_1 value of x at right end of shell

$\bar{x}$ dimensionless axial coordinate, x/y_o

$\bar{x}_1$ dimensionless length of shell, x_1/y_o

y shell radius; radial distance from shell axis of rotation to point on shell surface

$y' = \frac{dy}{dx}$

$y'' = \frac{d^2y}{dx^2}$

y_o value of y at $x = 0$ (see fig. 4)

$\bar{y}$ dimensionless shell radius, y/y_o

$\bar{y}' = \frac{d\bar{y}}{d\bar{x}}$

$\bar{y}'' = \frac{d^2\bar{y}}{d\bar{x}^2}$

$\bar{y}_o'$ slope of meridian at $x = 0$

ρ mass density of shell wall material

σ_c critical stress

$\sigma_{\phi,o}$ meridional stress at $x = 0$

σ_ϕ meridional stress

σ_θ circumferential stress

ϕ angle between tangent to shell meridian and a line parallel to shell axis (see fig. 4)

ϕ_o value of ϕ at $x = 0$

ω loading parameter, $2F_o/py_o$

DESCRIPTION OF PROBLEM

The minimum-mass design technique discussed in this report is applied to two classes of shell shapes: the transition section and the pressure-vessel head. The first shape to be examined is the transition section.

As used herein, a transition section is a shell of revolution which is used to join two other shells of revolution in such a way that all three shells have the same axis of revolution. An example is shown in figure 1. If the axis of revolution is identified as the X-axis, then the transition section extends from $x = 0$ to $x = x_1$. The transition section can be designed to support axisymmetric loadings such as normal pressure and axial loads. With respect to this first class of shell shapes, the problem is to determine the shape and thickness distribution for a minimum-mass transition section designed to support a given combination of pressure and axial load.

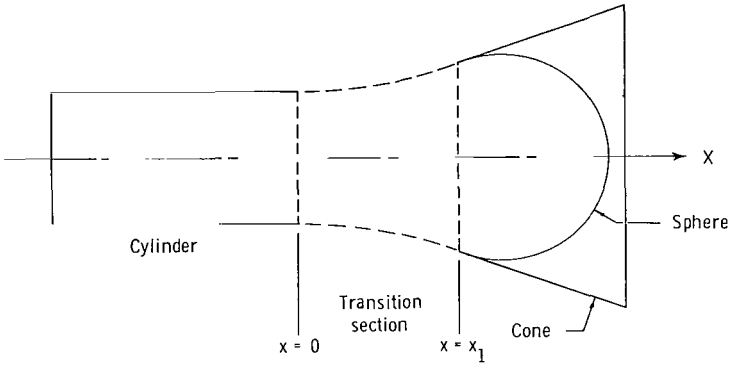

Figure 1.- Transition section joining a cylinder on the left with a sphere or cone on the right.

The second shape to be examined is the pressure-vessel head. The head is used as an end closure for an arbitrary shell of revolution. An example is shown in figure 2. Here the problem is to determine the shape and thickness distribution for a minimum-mass pressure-vessel head. This problem is complementary to the minimum-mass transition problem because combinations of minimum-mass transition sections and minimum-mass pressure-vessel heads provide complete, closed, minimum-mass shells.

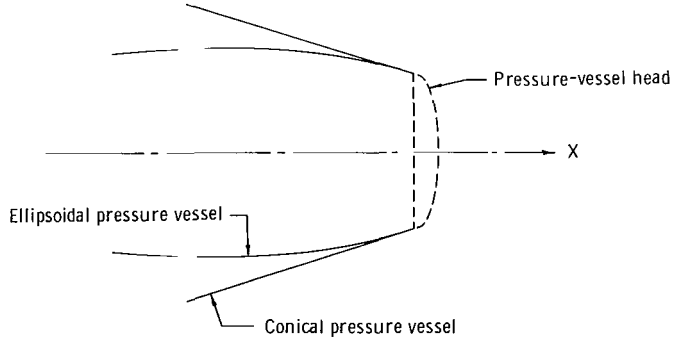

Figure 2.- Pressure-vessel head used as closure for a conical or ellipsiodal pressure vessel.

ANALYSIS

The mass m of a thin shell of revolution (see fig. 3) is given by

$$m = 2\rho\pi \int_{x=0}^{x=x_1} ty\sqrt{1 + (y')^2}\, dx \tag{1}$$

in which ρ is the density of the material (assumed constant), t is the thickness, and $y(x)$ is the curve which is rotated about the X-axis to generate the surface. It is

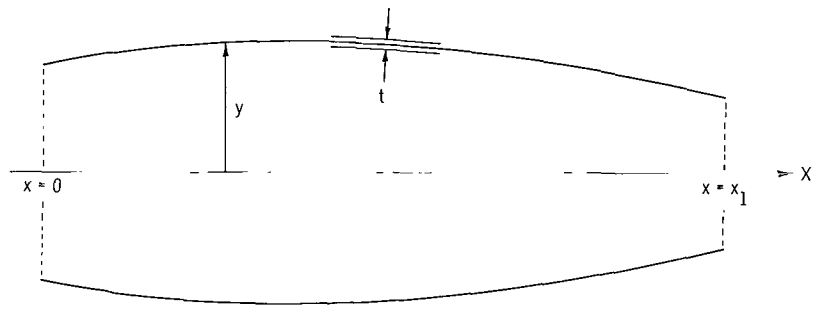

Figure 3.- General shell of revolution bounded by planes $x = 0$ and $x = x_1$.

necessary to express the thickness as a function of $y(x)$ and its derivatives and the type and intensity of loading. Such a relationship can be established by means of a critical stress condition and shell theory.

Critical Stress Condition

In this report it is assumed that the strain energy of distortion (Von Mises) yield condition is an adequate failure criterion. Without intending to dismiss as unimportant the problem of instability, buckling is not considered herein. The stresses at each point of the shell are thus related by

$$\sigma_1^2 - \sigma_1\sigma_2 + \sigma_2^2 = \sigma_c^2 \tag{2}$$

in which σ_1 and σ_2 are principal stresses and σ_c is some experimentally determined critical stress such as the yield stress. From linear membrane shell theory, if an axisymmetric stress condition is assumed, the principal stresses are given by

$$\sigma_1 = \frac{N_\theta}{t} \qquad \sigma_2 = \frac{N_\phi}{t} \tag{3}$$

so that

$$t = \frac{1}{\sigma_c}\left(N_\theta^2 - N_\theta N_\phi + N_\phi^2\right)^{1/2} \tag{4}$$

Loading and Stress Resultants

Consider an axisymmetric shell acted upon by a uniform hydrostatic pressure loading p and by some externally applied axial load per unit circumferential length, F_o, applied at $x = 0$ as shown in figure 4. Equilibrium of forces in the axial direction requires that the meridional stress σ_ϕ be given by

$$\sigma_\phi t 2\pi y \cos\phi = \sigma_{\phi,o} t_o 2\pi y_o \cos\phi_o + 2\pi p \int_{y_o}^{y} y\, dy \tag{5}$$

in which the subscript o is associated with points on the circumference of the shell at $x = 0$, and all other quantities are shown in figure 4.

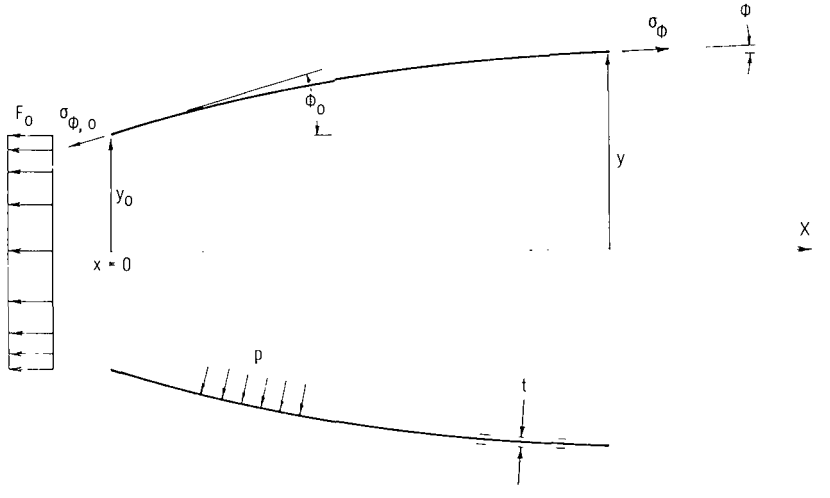

Figure 4.- Axisymmetric loading acting on shell of revolution.

The term "hydrostatic pressure" means that the pressure is applied to all surfaces of the shell, including the ends. It is assumed that pressure-vessel heads at axial locations beyond $x = 0$ and $x = x_1$ transmit the axial pressure load into the shell. The axial load per unit length of circumference, F_o, is an additional, externally applied load and is not directly associated with the pressure.

With this definition of hydrostatic pressure, it follows that the meridional stress $\sigma_{\phi,o}$ which appears in equation (5) is given by

$$\sigma_{\phi,o} t_o = \left(F_o + \frac{py_o}{2}\right)\frac{1}{\cos \phi_o} \tag{6}$$

A parameter ω which describes the loading is defined as

$$\omega = \frac{2\sigma_{\phi,o} t_o}{py_o} \cos \phi_o - 1 = \frac{2F_o}{py_o} \tag{7}$$

The loading parameter ω provides a convenient method for nondimensionalizing with respect to the pressure. It is the ratio of the externally applied axial load at $x = 0$ to the axial component of the pressure load at that same cross section. Since the pressure p can be internal (positive) or external (negative) and since F_o can be tensile (positive), zero, or compressive (negative), the parameter ω can be positive, zero, or negative. In defining the loading parameter ω in such a way that the pressure p is in the denominator, it is assumed that p is not zero. The case of $p = 0$ is handled separately as a special case.

From equations (5), (6), and (7), the stress σ_ϕ can be expressed as

$$\sigma_\phi t = N_\phi = \frac{py_o^2}{2y}\left(\omega + \frac{y^2}{y_o^2}\right)\sqrt{1 + (y')^2} \tag{8}$$

The equation of equilibrium of forces normal to the surface of the shell is

$$\frac{N_\phi}{R_1} + \frac{N_\theta}{R_2} = p \tag{9}$$

By making use of equations (8) and (9) and noting that

$$R_1 = -\frac{\left[1 + (y')^2\right]^{3/2}}{y''} \tag{10}$$

and

$$R_2 = y\sqrt{1 + (y')^2} \tag{11}$$

an expression for N_θ can be formed:

$$N_\theta = py\sqrt{1 + (y')^2} + \frac{py_o^2}{2}\left(\omega + \frac{y^2}{y_o^2}\right)\frac{y''}{\sqrt{1 + (y')^2}} \tag{12}$$

The following nondimensional barred quantities are introduced:

$$\bar{y} = \frac{y}{y_o} \tag{13}$$

$$\bar{x} = \frac{x}{y_o} \tag{14}$$

Then

$$y' = \bar{y}^{\cdot} \tag{15}$$

$$y'' = \frac{\bar{y}^{\cdot\cdot}}{y_o} \tag{16}$$

in which the primes denote differentiation with respect to x and the dots denote differentiation with respect to $\bar{x}$.

Nondimensional stress resultants $\overline{N}_\phi$ and $\overline{N}_\theta$ can be expressed in terms of the loading parameter ω and the nondimensional shape as follows:

$$\overline{N}_\phi \equiv \frac{2N_\phi}{py_o} = \frac{\omega + \bar{y}^2}{\bar{y}}\sqrt{1 + \left(\bar{y}^{\cdot}\right)^2} \tag{17}$$

$$\overline{N}_\theta \equiv \frac{2N_\theta}{py_o} = \frac{\left(\omega + \bar{y}^2\right)\bar{y}^{\cdot\cdot}}{\sqrt{1 + \left(\bar{y}^{\cdot}\right)^2}} + 2\bar{y}\sqrt{1 + \left(\bar{y}^{\cdot}\right)^2} \tag{18}$$

A nondimensional thickness $\bar{t}$ can be expressed as

$$\bar{t} \equiv \frac{2t\sigma_c}{py_o} = \left(\overline{N}_\phi^{\,2} - \overline{N}_\theta\overline{N}_\phi + \overline{N}_\theta^{\,2}\right)^{1/2} \tag{19}$$

By using equation (1), with equation (19) relating the thickness to the stress resultants and equations (17) and (18) relating the stress resultants to the geometry and loading, the nondimensional mass $\overline{m}$ can be expressed as

$$\overline{m} \equiv \frac{m\sigma_c}{\pi\rho p y_o^{\,3}} = \int_{\bar{x}=0}^{\bar{x}=\bar{x}_1} \bar{t}\,\bar{y}\sqrt{1 + \left(\bar{y}^{\cdot}\right)^2}\,d\bar{x} \tag{20}$$

In the special case for which the pressure p is zero, the following equations apply:

$$N_\phi = \frac{F_o\sqrt{1 + \left(\bar{y}^{\cdot}\right)^2}}{\bar{y}} \tag{21}$$

$$N_\theta = \frac{F_o\bar{y}^{\cdot\cdot}}{\sqrt{1 + \left(\bar{y}^{\cdot}\right)^2}} \tag{22}$$

The thickness is calculated from equation (4) and the mass is calculated from equation (1).

As formulated in equation (20) the shell wall thickness varies along the meridian. Minimum-mass shells of uniform thickness can be generated by basing the thickness upon

the average stress condition in the shell or upon the most critical stress condition in the shell. (See, for example, refs. 10 and 11.) The present report considers only those shells for which the thickness varies along the meridian.

A method for obtaining the shell shape $\bar{y}(\bar{x})$ which minimizes $\overline{m}$ is presented after the required boundary conditions are examined.

Boundary Conditions

The number and types of boundary conditions which are appropriate to this optimization problem can be obtained by use of the calculus of variations. Let equation (20) be written as

$$\overline{m} = \int_{\bar{x}=0}^{\bar{x}=\bar{x}_1} f\left(\bar{y},\bar{y}^{\cdot},\bar{y}^{\cdot\cdot}\right)d\bar{x} \tag{23}$$

where, from equations (17) to (20), f is given by

$$f = \left\{ \frac{\left(\omega + \bar{y}^2\right)^2\left[1 + \left(\bar{y}^{\cdot}\right)^2\right]}{\bar{y}^2} - \frac{\left(\omega + \bar{y}^2\right)^2\bar{y}^{\cdot\cdot}}{\bar{y}} - 2\left(\omega + \bar{y}^2\right)\left[1 + \left(\bar{y}^{\cdot}\right)^2\right] + \frac{\left(\omega + \bar{y}^2\right)^2\left(\bar{y}^{\cdot\cdot}\right)^2}{1 + \left(\bar{y}^{\cdot}\right)^2} \right.$$

$$\left. + 4\bar{y}\bar{y}^{\cdot\cdot}\left(\omega + \bar{y}^2\right) + 4\bar{y}^2\left[1 + \left(\bar{y}^{\cdot}\right)^2\right] \right\}^{1/2} \bar{y}\sqrt{1 + \left(\bar{y}^{\cdot}\right)^2} \tag{24}$$

The variational equation for the functional $\overline{m}\left[\bar{y}(\bar{x})\right]$ is of the form

$$\delta\overline{m} = \int_{\bar{x}=0}^{\bar{x}=\bar{x}_1}\left[\left(\frac{\partial f}{\partial \bar{y}}\right)\delta\bar{y} + \left(\frac{\partial f}{\partial \bar{y}^{\cdot}}\right)\delta\bar{y}^{\cdot} + \left(\frac{\partial f}{\partial \bar{y}^{\cdot\cdot}}\right)\delta\bar{y}^{\cdot\cdot}\right]d\bar{x} = 0 \tag{25}$$

In order to examine the types of boundary conditions that are required, the second term in the integrand is integrated by parts once and the third term is integrated by parts twice to give

$$\delta\overline{m} = \left\{\left[\frac{\partial f}{\partial \bar{y}^{\cdot}} - \frac{d}{d\bar{x}}\left(\frac{\partial f}{\partial \bar{y}^{\cdot\cdot}}\right)\right]\delta\bar{y}\right\}_{\bar{x}=0}^{\bar{x}=\bar{x}_1} + \left[\left(\frac{\partial f}{\partial \bar{y}^{\cdot\cdot}}\right)\delta\bar{y}^{\cdot}\right]_{\bar{x}=0}^{\bar{x}=\bar{x}_1}$$

$$+ \int_{\bar{x}=0}^{\bar{x}=\bar{x}_1}\left[\frac{\partial f}{\partial \bar{y}} - \frac{d}{d\bar{x}}\left(\frac{\partial f}{\partial \bar{y}^{\cdot}}\right) + \frac{d^2}{d\bar{x}^2}\left(\frac{\partial f}{\partial \bar{y}^{\cdot\cdot}}\right)\right]\delta\bar{y}\,d\bar{x} = 0 \tag{26}$$

The boundary conditions which are given in equation (26) are:

At $\bar{x} = 0$,

$$\frac{\partial f}{\partial \bar{y}'} - \frac{d}{dx}\left(\frac{\partial f}{\partial \bar{y}''}\right) = 0 \qquad \text{or } \bar{y} \text{ prescribed} \tag{27}$$

$$\frac{\partial f}{\partial \bar{y}''} = 0 \qquad \text{or } \bar{y}' \text{ prescribed} \tag{28}$$

At $\bar{x} = \bar{x}_1$,

$$\frac{\partial f}{\partial \bar{y}'} - \frac{d}{dx}\left(\frac{\partial f}{\partial \bar{y}''}\right) = 0 \qquad \text{or } \bar{y} \text{ prescribed} \tag{29}$$

$$\frac{\partial f}{\partial \bar{y}''} = 0 \qquad \text{or } \bar{y}' \text{ prescribed} \tag{30}$$

These are all the legitimate choices for boundary conditions. The boundary conditions that are used in the examples presented in this report are the prescription of $\bar{y}$ and $\bar{y}'$ at each end.

For the case of $\omega = -1.0$, examination of equation (24) shows that $\partial f / \partial \bar{y}''$ is zero at $\bar{x} = 0$ $\left(\text{since } \bar{y}_o = \frac{y_o}{y_o} = 1.0\right)$. Therefore, from equation (28), the slope $\bar{y}'$ cannot be prescribed at that end. Note that when $\omega = -1.0$ the externally applied axial load at $\bar{x} = 0$ cancels the axial component of the pressure load at the same end so that $\bar{N}_\phi$ is zero there. Thus, equilibrium can be maintained even if a slope discontinuity exists.

It is emphasized here that deflections and deformations are not considered in this report. The coordinate and slope boundary conditions refer to the shell shape at the ends and do not refer to deflections away from some initial shape.

MINIMIZATION OF MASS BY THE RITZ PROCEDURE AND NONLINEAR PROGRAMING METHODS

The problem of finding the shape and thickness distribution of a minimum-mass shell of revolution has been cast in the form of finding the function $y(x)$ which minimizes a functional of the form $\int f(y,y',y'')dx$. In this report Ritz's method, together with nonlinear programing techniques, is used in the minimization.

Two types of shell shapes are considered. The first type is denoted transition section. For this type of shape, the shell radius $\bar{y}$ is not zero at either end. The second type of shell shape is the pressure-vessel head.

Transition Sections

The examples for transition sections presented in this report include only shapes that are symmetric about the midlength $\bar{x}_1/2$. An equation which can be used to describe any smooth transition section of this type is

$$\bar{y} = 1 + \bar{y}_o'\left(\bar{x} - \frac{\bar{x}^2}{\bar{x}_1}\right) + \sum_{n=1,2,3}^{\infty} c_n \sin^2 \frac{n\pi\bar{x}}{\bar{x}_1} \tag{31}$$

The first two terms on the right-hand side of equation (31) are used to satisfy the required coordinate and slope boundary conditions. The factor $\bar{y}_o'$ is the slope at $\bar{x} = 0$. The constants c_n are used to minimize the mass. The trigonometric series can describe any smooth curve that is symmetric about the midlength and that has zero coordinate and slope boundary conditions. Regardless of the values of c_n the trigonometric series makes no contribution to the coordinate and slope boundary conditions that are applied to the transition section.

Although the transition sections presented in this report are limited to shapes that are symmetric about the midlength, a more general expression which could be used to generate unsymmetric shapes is

$$\bar{y} = 1 + a_1\bar{x} + a_2\bar{x}^2 + a_3\bar{x}^3 + \sum_{n=0,1,2}^{\infty} c_n\left[\cos \frac{n\pi\bar{x}}{\bar{x}_1} - \cos \frac{(n+2)\pi\bar{x}}{\bar{x}_1}\right] \tag{32}$$

The constants a_1, a_2, and a_3 are used to satisfy the boundary conditions.

Pressure-Vessel Heads

The pressure-vessel heads considered herein act as closures for axisymmetric but otherwise arbitrarily shaped pressure vessels. At the junction of the head and vessel the coordinates and slope of the pressure-vessel head are assumed to match those of the pressure vessel. All loads acting on the pressure-vessel head are assumed to result from uniform hydrostatic pressure; therefore the loading parameter ω is zero. But this requirement on ω does not extend to the pressure vessel to which the head is attached. The pressure vessel can carry an externally applied axial load, as shown in figure 5.

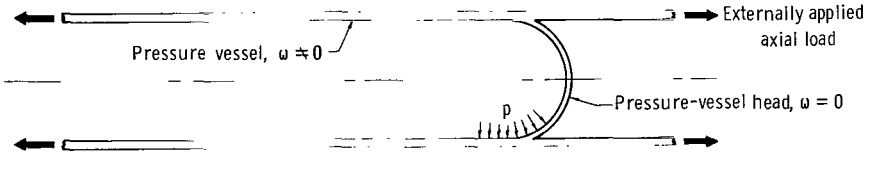

Figure 5.- Pressure-vessel head attached to cylindrical pressure vessel which is carrying an externally applied axial load.

An expression for $\bar{y}(\bar{x})$ which can satisfy the boundary conditions and which forms a smooth closure for a pressure vessel may be written as

$$\bar{y} = \sum_{n=0,1,2}^{\infty} c_n \left(1 - \frac{\bar{x}}{\bar{b}}\right)^{n+\frac{1}{2}} \tag{33}$$

in which $\bar{b}$ is the dimensionless depth of the head. Two of the arbitrary coefficients are used to satisfy the coordinate and slope boundary conditions at $\bar{x} = 0$, the junction of the head and vessel. The remaining coefficients and the depth of the head are used to minimize the mass.

The series given in equation (33) was chosen because it provides smooth stresses at $\bar{x} = \bar{b}$, the apex of a pressure-vessel head. Mathematically the smooth-stress criterion is given by

$$\lim_{\bar{x} \to \bar{b}} \frac{d\bar{N}_\theta}{d\bar{s}} = 0 \tag{34}$$

and

$$\lim_{\bar{x} \to \bar{b}} \frac{d\bar{N}_\phi}{d\bar{s}} = 0 \tag{35}$$

where $\bar{s}$ is the dimensionless distance along the meridian.

Equations (34) and (35) guarantee that the thickness is also smooth at the apex – that is,

$$\lim_{\bar{x} \to \bar{b}} \frac{d\bar{t}}{d\bar{s}} = 0 \tag{36}$$

Nonlinear Programing Methods

The values of c_n in equations (31) and (33) were obtained by nonlinear programing methods. The c_n are the design variables and the mass $\bar{m}$ is the objective function. The direction-generating algorithms that were used include random, gradient, sectioning, Newton-Raphson, and Fletcher-Powell. After the direction-generating algorithm was used to calculate a set of direction cosines for a move, a one-dimensional search was carried out to find the minimum-mass design in that direction.

In the random method the direction cosines are generated from random numbers. In the gradient method the move direction is the negative gradient direction. In the sectioning method the design variables are improved sequentially rather than simultaneously. As used in this report, the Newton-Raphson method (ref. 16) searches for the c_n that are solutions to the set of equations $\frac{\partial \bar{m}}{\partial c_n} = 0$. The Fletcher-Powell method is described in references 17 to 20.

The computer program was written in such a way that several direction-generating methods could be used in a single computer run. Several methods were used to start designs. The Fletcher-Powell method was used to complete all designs having 10 or more design variables c_n.

RESULTS AND DISCUSSION

Transition Sections

Linear membrane shell theory, the Von Mises yield condition, and equation (31) were used to generate typical minimum-mass shapes and thickness distributions for transition sections having four combinations of geometric end conditions, all of which are symmetric with respect to the midlength. One transition section has a length equal to the radius at each end and has zero-slope end conditions. Another transition section has a length equal to 1.5 times the radius at each end and has zero-slope end conditions. A third transition section has a length equal to 1.5 times the radius at each end; the slope at the left end is 0.5 and the slope at the right end is -0.5. The fourth transition section is a special case ($\omega = -1.0$) for which the slopes at the ends cannot be prescribed in advance. For this fourth transition section, the length is 1.5 times the radius at each end. Results are shown in figures 6 to 19.

The discussion of transition sections includes, first, a presentation of shapes, thickness distributions, and stress resultants. Next, certain aspects of these results are examined. Finally, an indication of potential mass savings is presented.

Shapes, thickness distributions, and stress resultants.- Three slope end conditions are considered: (1) zero-slope end conditions, (2) nonzero-slope end conditions, and (3) the special case $\omega = -1.0$ for which the slopes at the ends cannot be prescribed.

(1) Transition sections with zero-slope end conditions: The transition sections shown in figure 6 have a nondimensional length $\bar{x}_1$ equal to 1.0, which means that the length is equal to the radius at each end. The nondimensional meridional shapes for several values of ω are shown in figure 6(a). All these shapes neck down in the center except for the limiting cases $\omega = \pm\infty$ ($p = 0$), which are cylinders.

The nondimensional thickness distributions associated with three of the preceding shapes, $\omega = 0.6$, 0.0, and -0.4, are shown in figure 6(b). The thickness for the cases $\omega = \pm\infty$ ($p = 0$) can be calculated from equation (4). The thickness distributions are discussed in more detail in a subsequent section entitled "Oscillations in the thickness distribution."

The nondimensional meridional and circumferential stress resultants are shown in figures 6(c) and 6(d), respectively. Note that the thickness distributions shown in

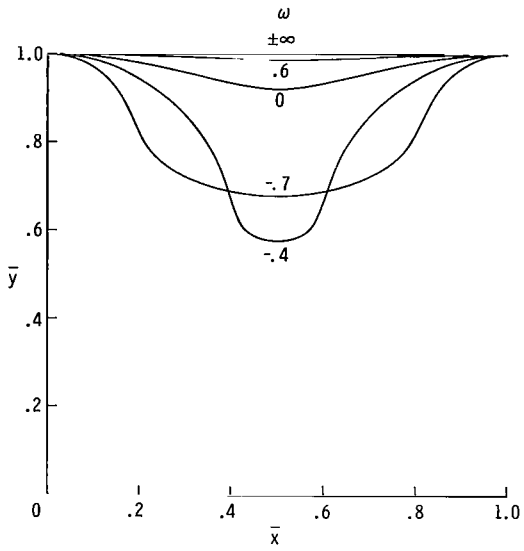

(a) Nondimensional meridional shape.

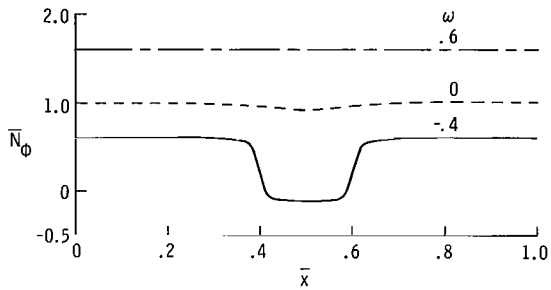

(c) Nondimensional meridional stress resultant.

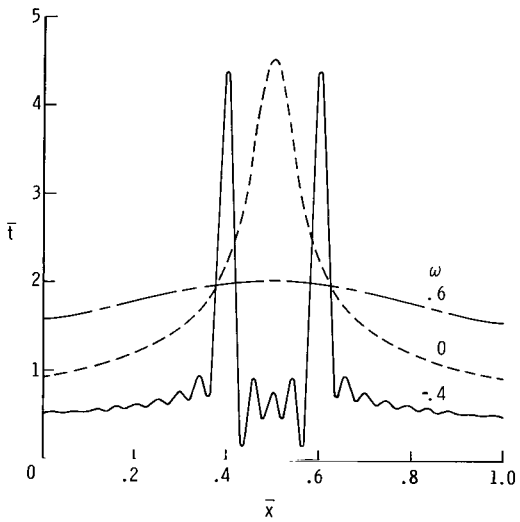

(b) Nondimensional thickness distribution.

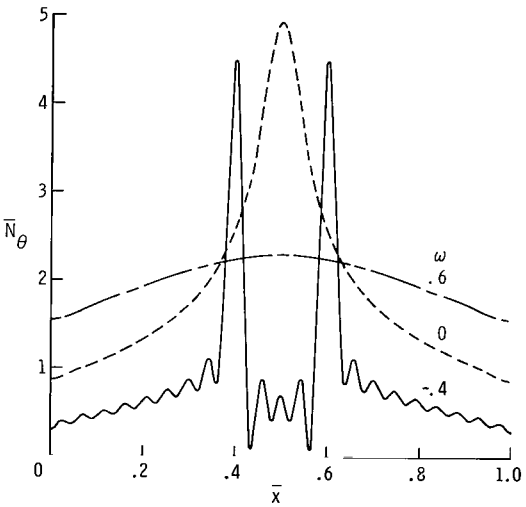

(d) Nondimensional circumferential stress resultant.

Figure 6.- Nondimensional meridional shapes, thickness distributions, and stress resultants for several minimum-mass transition sections with $\bar{x}_1 = 1.0$ and $\bar{y}'_o = 0$.

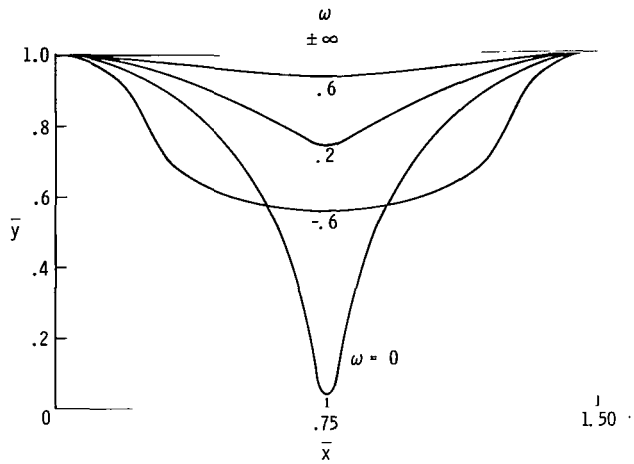

(a) Nondimensional meridional shape.

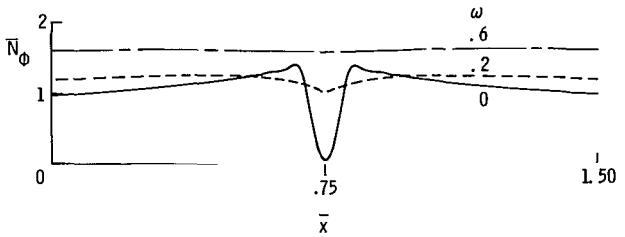

(c) Nondimensional meridional stress resultant.

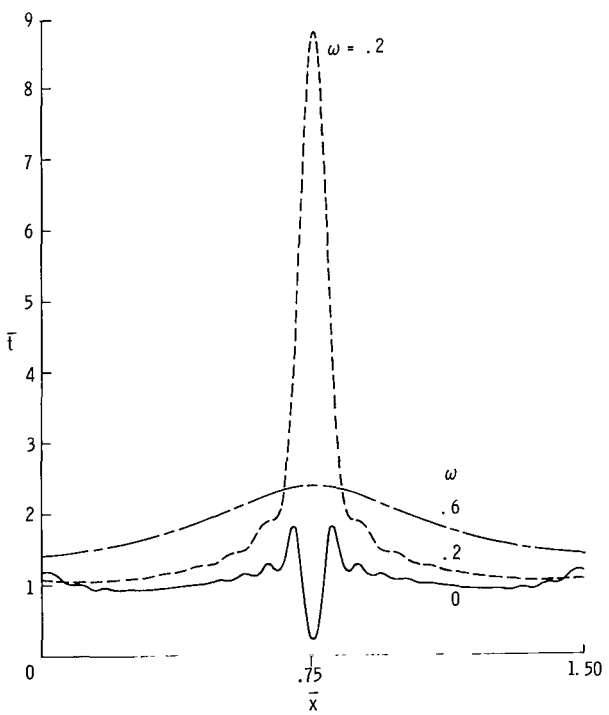

(b) Nondimensional thickness distribution.

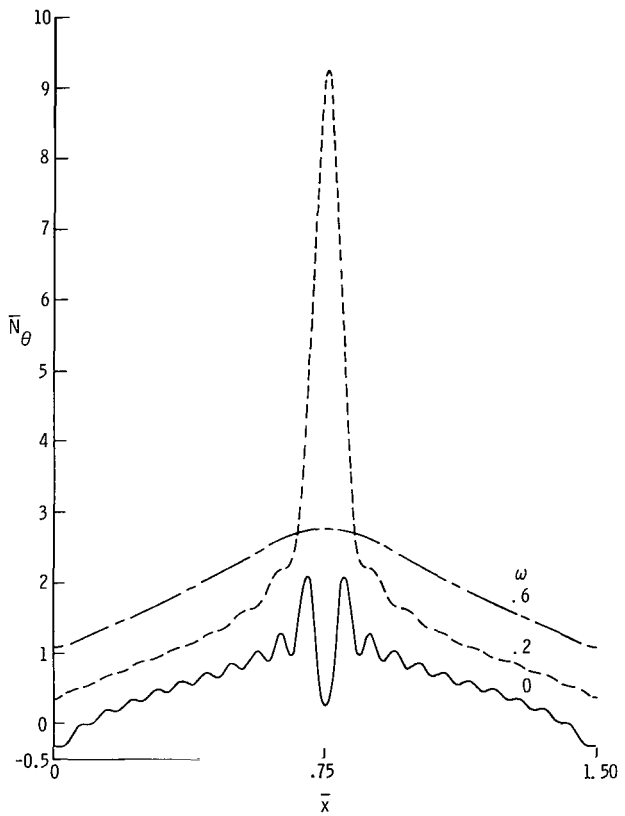

(d) Nondimensional circumferential stress resultant.

Figure 7.- Nondimensional meridional shapes, thickness distributions, and stress resultants for several minimum-mass transition sections with $\bar{x}_1 = 1.5$ and $\bar{y}_o = 0$.

figure 6(b) reflect the stress distributions shown in figure 6(d). The stress resultants for $\omega = \pm\infty$ can be calculated from equations (21) and (22).

The transition sections shown in figure 7 have a nondimensional length $\bar{x}_1$ equal to 1.5 and have zero-slope end conditions. This set of transition sections is therefore similar to, but 50 percent longer than, the set of figure 6. The increase in length allows these minimum-mass designs to neck down in the center more than the previous set.

The shell radius $\bar{y}$ at the midlength $\bar{x}_1/2$ of both sets of transition sections is shown as a function of the loading parameter ω in figure 8. The upper curve is for the transition sections having $\bar{x}_1 = 1.0$, and the lower curve is for the transition sections having $\bar{x}_1 = 1.5$. For these two sets of transition sections the midlength point is the point at which the minimum value of $\bar{y}$ occurs. Hence, these curves show the minimum value of $\bar{y}$ as a function of ω. The symbols indicate calculated designs. The transition sections having $\bar{x}_1 = 1.0$ are essentially cylindrical for $\omega > 1.0$ and $\omega < -3.0$. The transition sections with $\bar{x}_1 = 1.5$ neck down for a wider range of ω and are essentially cylindrical for $\omega > 2.0$ and $\omega < -4.0$.

(2) Transition sections with non-zero-slope end conditions: The shapes, thickness distributions, and stress distributions for several transition sections having non-zero-slope end conditions are shown in figure 9. For these transition sections the slope at the left end is 0.5 and the slope at the right end is -0.5. The nondimensional length $\bar{x}_1$ is 1.5. Except for the slopes at the ends of the meridional shapes, the results shown in figure 9 are similar to the results shown in figures 6 and 7.

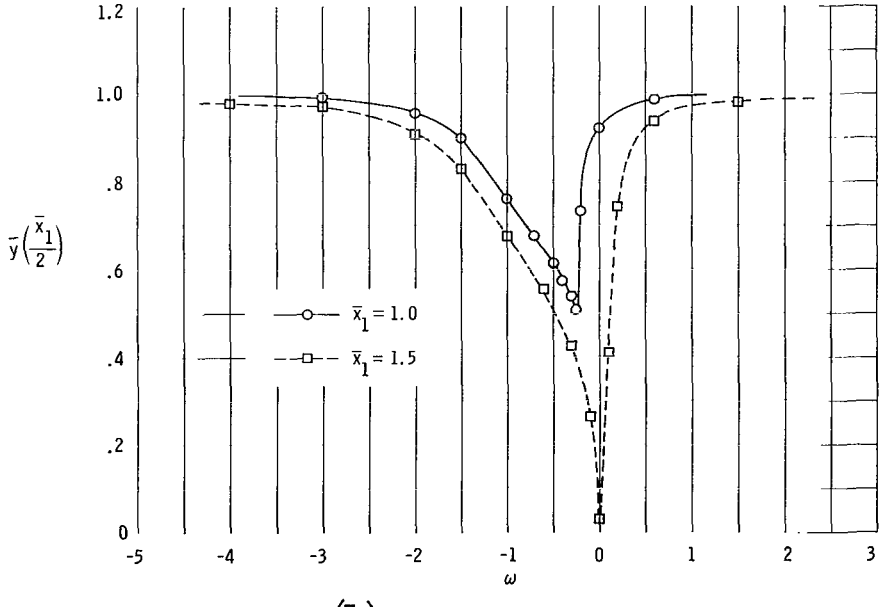

Figure 8.- Midlength radius $\bar{y}\left(\frac{\bar{x}_1}{2}\right)$ as a function of loading parameter ω for two types of transition sections with zero-slope end conditions.

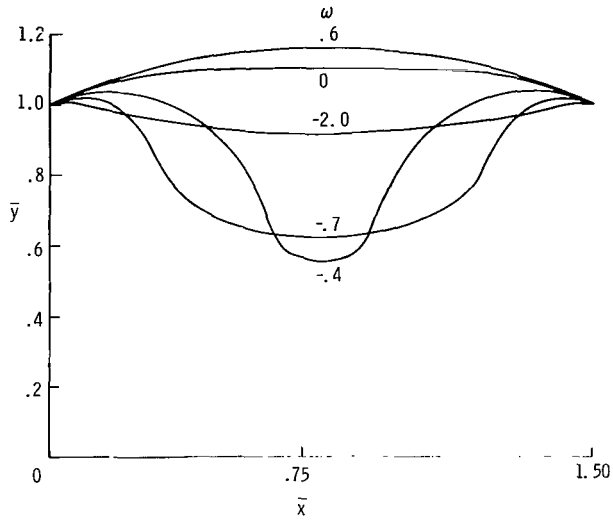

(a) Nondimensional meridional shape.

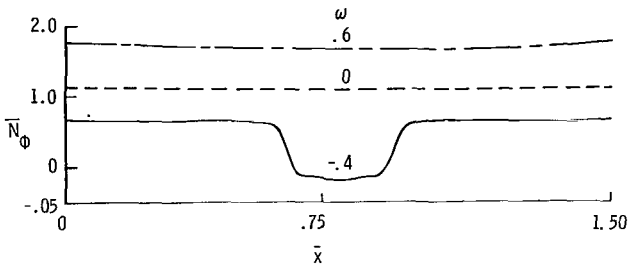

(c) Nondimensional meridional stress resultant.

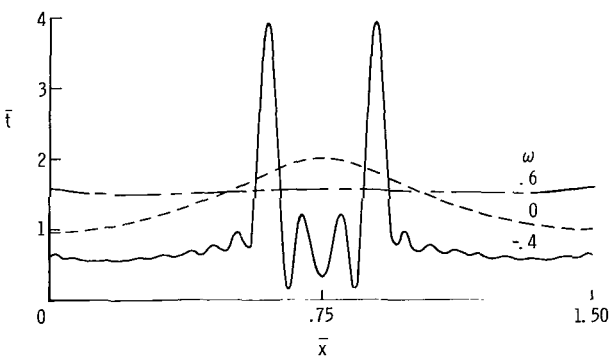

(b) Nondimensional thickness distribution.

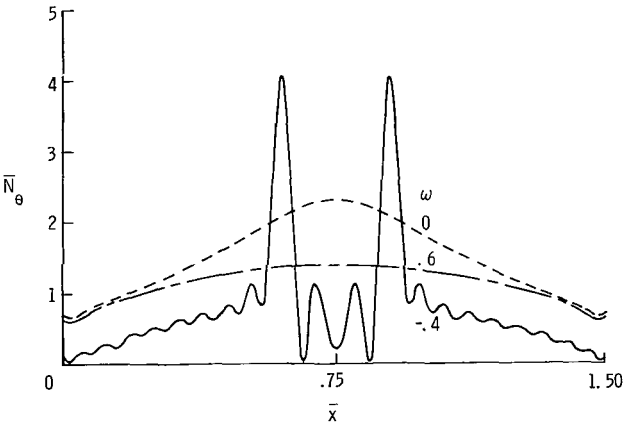

(d) Nondimensional circumferential stress resultant.

Figure 9.- Nondimensional meridional shapes, thickness distributions, and stress resultants for several minimum-mass transition sections with $\bar{x}_1 = 1.5$ and $\bar{y}_o = 0.5$.

For transition sections having the same length and end conditions as those of figure 9, the shell radius $\bar{y}$ at the midlength $\bar{x}_1/2$ is shown as a function of the loading parameter ω in figure 10. The symbols indicate calculated designs.

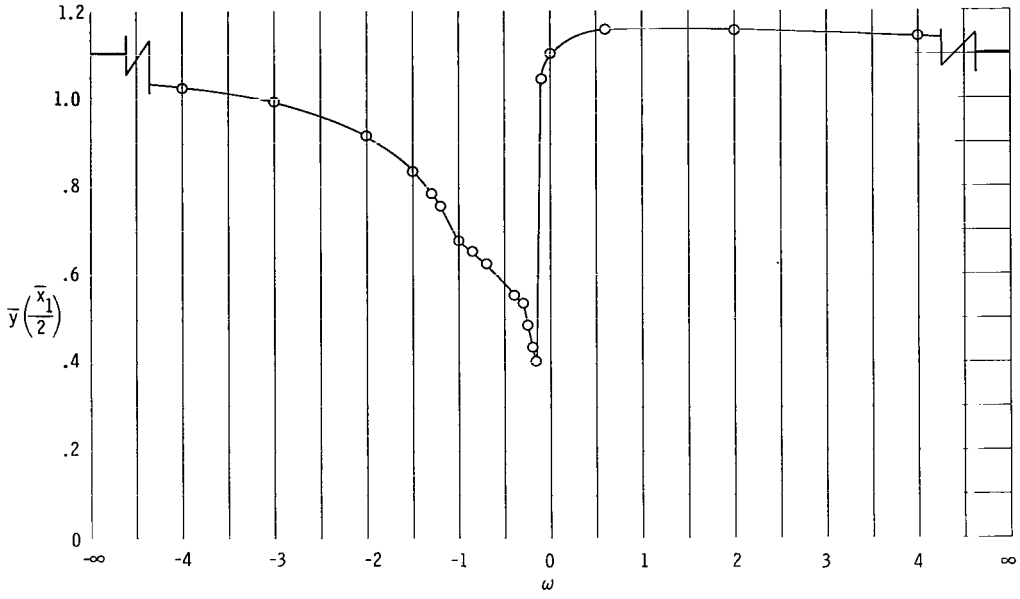

Figure 10.- Midlength radius $\bar{y}\left(\frac{\bar{x}_1}{2}\right)$ as a function of loading parameter ω for transition sections with $\bar{x}_1 = 1.5$ and $\bar{y}_o' = 0.5$.

The special case for which the pressure p is zero is presented in figure 11. The very great thickness at the ends suggests that a ring may be useful at each end of the shell.

(3) The special case $\omega = -1.0$: As was stated previously in the section entitled "Boundary Conditions," when the loading parameter ω is equal to -1.0 the slope boundary condition cannot be prescribed at the left end $\bar{x} = 0$. Since the examples for transition sections presented in this report include only shapes that are symmetric about the midlength, the restriction concerning slope boundary conditions applies to the right end $\bar{x} = \bar{x}_1$ as well as to the left end. The restriction on prescription of slope boundary conditions means that in addition to minimizing the mass with respect to the c_n in equation (31), the mass must also be minimized with respect to $\bar{y}_o'$.

An example of a transition section for which $\omega = -1.0$ and $\bar{x}_1 = 1.5$ is shown in figure 12. For this design $\bar{y}_o' = -2.784$. The design appears to require rings or bands at the ends and a relatively uniform wall thickness over the rest of the shell. The midlength radius $\bar{y}\left(\bar{x}_1/2\right)$ for two cases with $\omega = -1.0$ is also included in figures 8 and 10.

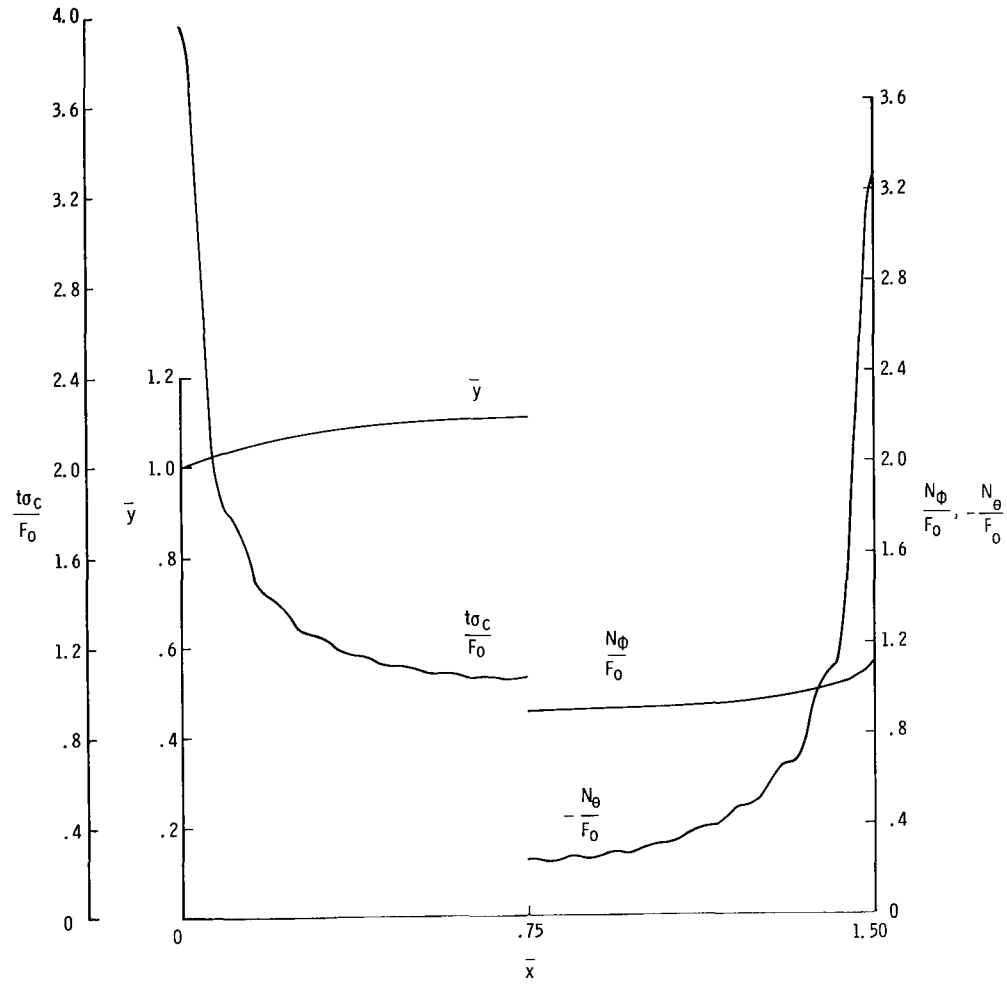

Figure 11.- Meridional shape, thickness distribution, and stress resultants for minimum-mass transition section carrying only an axial load F_o, with $\bar{x}_1 = 1.5$ and $\bar{y}_o = 0.5$.

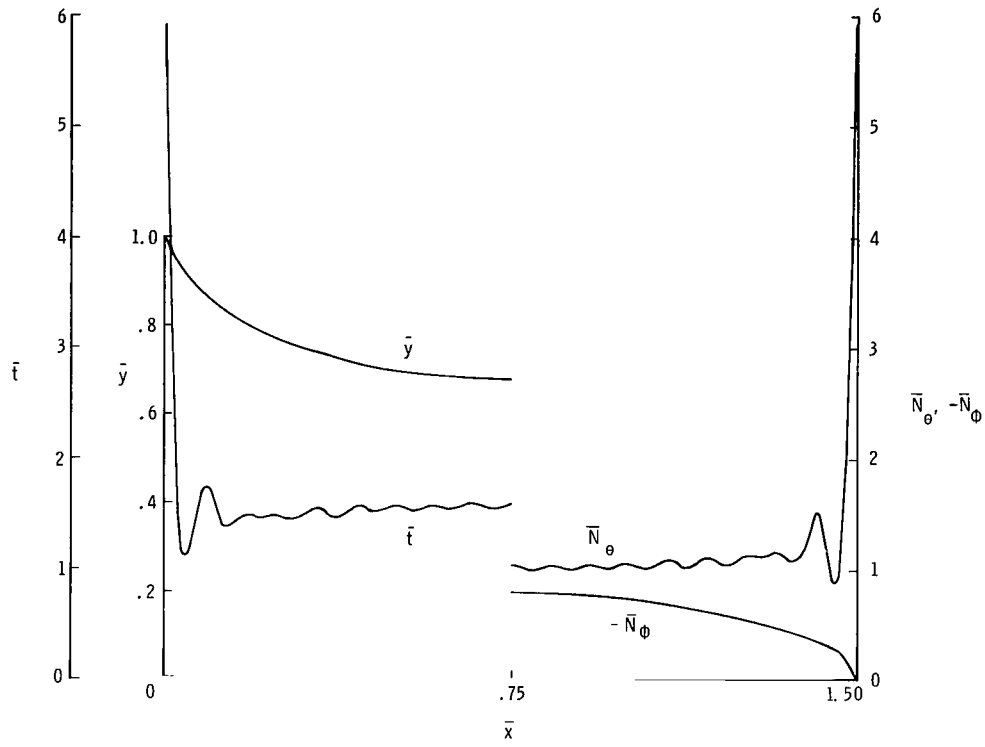

Figure 12.- Meridional shape, thickness distribution, and stress resultants for minimum-mass transition section with $\omega = -1.0$, $\bar{x}_1 = 1.5$, and end slopes not prescribed.

Numerical values of the masses and Ritz coefficients (or design variables) c_n are given in tables I(a), I(b), I(c), II, and III for the shell shapes presented in figures 6, 7, 9, 11, and 12, respectively.

Oscillations in the thickness distribution.- The oscillatory character of some of the thickness distributions (for example, see $\omega = -0.4$ in fig. 6(b)) arises because a series solution is used. For practical construction the oscillatory thickness distributions would have to be smoothed in some manner. Part of the problem may arise because the shell shape, rather than the shell thickness, is being expressed as a series. The thickness is obtained by differentiating this series – a procedure that is known to cause convergence problems in some instances. For this reason, it is interesting to see how the thickness distribution changes as the number of terms in the shape series is changed.

Curves which show these changes for the case $\omega = -0.4$ of figure 6(b) are presented in figure 13. Because of symmetry, only half the shell is shown. It appears that certain trends in the thickness distribution have been established. From $\bar{x} = 0$ to $\bar{x} = 0.35$, the thickness could be smoothed to provide a slowly changing thickness; at $\bar{x} = 0.40$ a large peak in the thickness occurs. The mass of the 10-term solution is less

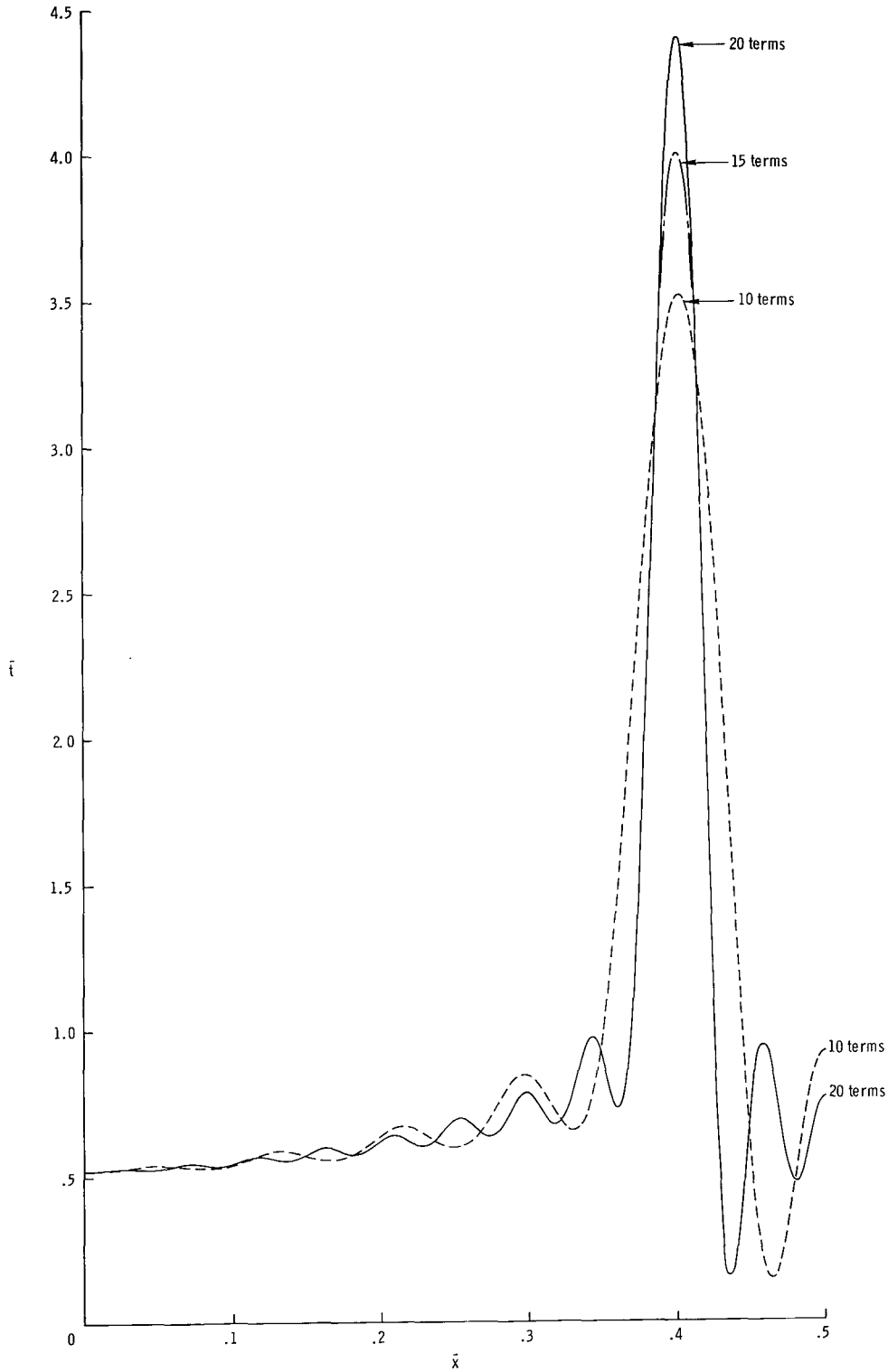

Figure 13.- Nondimensional thickness distribution for 10-term, 15-term, and 20-term shape series with $\bar{x}_1 = 1.0$, $\bar{y}_o^{\cdot} = 0$, and $\omega = -0.4$.

than 2 percent more than the mass of the 20-term solution, and the mass of the 15-term solution is less than 0.5 percent more than the mass of the 20-term solution. The corresponding changes in the values of $\bar{y}$ at the midlength of the shell are also small. If only the shell shape and the objective function, which is the mass, are considered, the series has converged. However, additional terms cause substantial changes in the thickness distribution. Perhaps including even more terms in the series would cause the oscillatory character of the thickness distribution to disappear eventually, but the short-wavelength terms which would be added would allow the large peak at $\bar{x} = 0.40$ to become higher and narrower. In cases such as this, constraints may be imposed to obtain a more practical solution.

Negative (compressive) stresses, buckling, and constraints.- In the procedures discussed in the preceding pages the critical stress condition used has been the Von Mises yield condition, and the possibility of buckling has not been considered even though compressive stresses may be present in the shell wall. For many loadings and boundary conditions it is possible, in designing the shell, to use an inequality constraint which eliminates compressive stresses. In other cases, constraints could be used to prevent sharp peaks in a stress or thickness distribution and to prevent the shell shape from necking down more than a prescribed amount. In this section two examples of constrained solutions are presented. Both are for the $\omega = -0.4$ case of figure 6, and in both examples a stress resultant constraint is imposed.

In the first example, $\overline{N}_\theta$ is required to be less than 2.5. The constraint is imposed in an attempt to reduce or remove the spikes which occur in the $\overline{N}_\theta$ distribution at $\bar{x} = 0.4$ and $\bar{x} = 0.6$. For comparison, $\overline{N}_\theta = 2.0$ for a cylinder. The results are presented in figure 14. The constraint turns out to be quite severe. Whereas the unconstrained solution is 29 percent lighter than the corresponding cylinder having the same length and end radius and subjected to the same loading, the constrained solution is only 12 percent lighter than the cylinder. The mass and Ritz coefficients are given in table IV(a).

In the second example, $\overline{N}_\phi$ is required to be positive (tensile, for internal pressure) over the total length of the shell. In the unconstrained solution, $\overline{N}_\phi$ is negative at the center. The results, which were obtained from a 15-term solution, are presented as solid lines in figure 15. Portions of the shape, thickness, and stress resultants for the 15-term unconstrained design are shown in figure 15 as dashed lines. In this case the constraint is not severe. The constrained solution which has no negative stresses is 26 percent lighter than the cylinder, whereas the unconstrained solution is 29 percent lighter than the cylinder. The mass and Ritz coefficients are given in table IV(b).

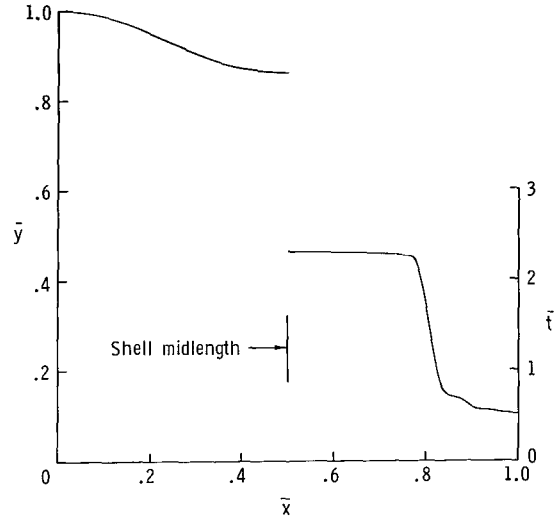

(a) Nondimensional meridional shape and thickness distribution.

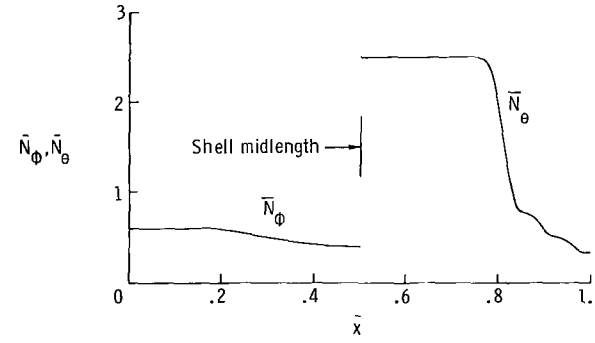

(b) Nondimensional stress resultants.

Figure 14.- Nondimensional meridional shape, thickness distribution, and stress resultants for minimum-mass transition section with $\bar{x}_1 = 1.0$, $\bar{y}_o = 0$, $\omega = -0.4$, and the added constraint $\bar{N}_\theta < 2.5$.

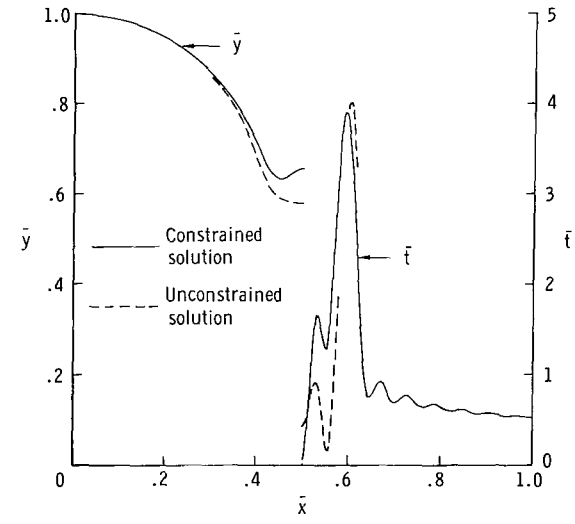

(a) Nondimensional meridional shapes and thickness distribution.

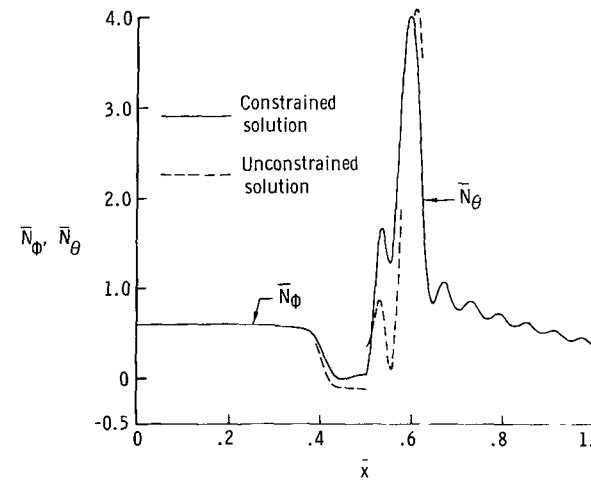

(b) Nondimensional stress resultants.

Figure 15.- Nondimensional meridional shapes, thickness distributions, and stress resultants for a minimum-mass shell designed to have no negative stresses and for the minimum-mass shell having the same loading and boundary conditions but designed without that constraint. $\bar{x}_1 = 1.0$; $\bar{y}_o = 0$; $\omega = -0.4$.

In both of these examples the constraint was imposed by the sequential unconstrained minimization technique (SUMT) method of references 21 and 22, which makes use of a penalty function. Additional information on the use of the SUMT method in structural optimization problems may be found in references 18, 19, and 20.

Bending stresses.- Since bending stresses are neglected in the development of these minimum-mass shell shapes and thickness distributions, it is of interest to determine whether the stress distributions predicted by bending theory are significantly different from those predicted by membrane theory. Stresses at the inner and outer surfaces of the shell were therefore calculated by using a computer program based on linear bending shell theory (ref. 23) for the case $\omega = 0.2$ of figure 7.

The end radius y_o chosen for the shell is 10 in. (25.4 cm) and the length x_1 is therefore 15 in. (38.1 cm). The shell is assumed to be fabricated of a steel which has the following properties: modulus of elasticity $E = 30 \times 10^3$ ksi (207 GN/m^2); yield stress $\sigma_c = 35$ ksi (241 MN/m^2); Poisson's ratio, 0.3. The boundary conditions used at each end of the shell are: no restraint against normal displacement and no restraint against meridional rotation.

The results are presented in figure 16. The stress quantity $\sqrt{\sigma_\theta^2 - \sigma_\theta\sigma_\phi + \sigma_\phi^2}$ at the inner and outer surface of the shell wall is shown as a function of arc length

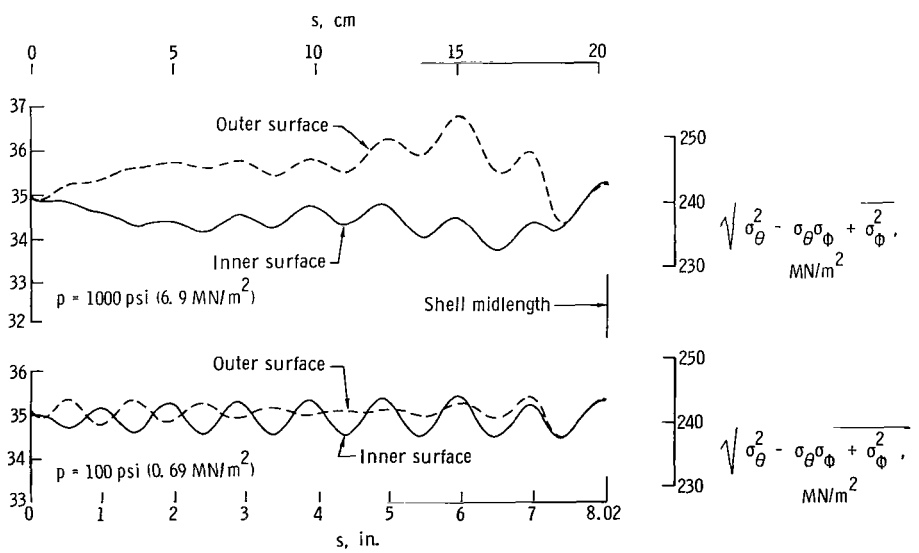

Figure 16.- The stress quantity $\sqrt{\sigma_\theta^2 - \sigma_\theta\sigma_\phi + \sigma_\phi^2}$ at the inner and outer surfaces of two minimum-mass transition sections as a function of distance s measured along meridian. $y_o = 10$ in. (25.4 cm); $x_1 = 15$ in. (38.1 cm); $y_o' = 0$; $\omega = 0.2$.

measured along the shell for two values of internal pressure p. The amount by which this stress quantity differs from 35 ksi (241 MN/m^2) represents the inadequacy of linear membrane theory for that loading. The curves show that for low loadings (p = 100 psi (0.69 MN/m^2)) membrane theory is adequate and that for high loadings (p = 1000 psi (6.9 MN/m^2)) membrane theory is marginal. The dimensional thickness distribution can be calculated by using y_o = 10 in. (25.4 cm) and σ_c = 35 ksi (241 MN/m^2) in equation (19) together with the thickness distribution $\bar{t}$ shown in figure 7(b) for ω = 0.2. For p = 1000 psi (6.9 MN/m^2) the thickness at the center is 1.3 in. (3.3 cm) and for p = 100 psi (0.69 MN/m^2) the thickness at the center is 0.13 in. (0.33 cm).

The thickness distribution for p = 1000 psi (6.9 MN/m^2) was simplified as shown in figure 17 and the shell was reanalyzed. The stress quantity at the inner and outer surfaces of the modified shell is presented in figure 18 as a function of the arc length measured along the shell. The stress quantity remains below the yield stress for the entire shell. The dimensionless mass $\bar{m}$ for the original, unmodified shell is 2.35. The thickness simplification increases $\bar{m}$ to 2.58.

Mass saving.- An indication of the mass saving that can be realized by using the present method is shown in figure 19. For the transition sections shown in figures 6 and 7 the ratio of the mass m to the mass of uniform-thickness cylinders designed to carry the same load is presented in figure 19 as a function of the loading parameter ω.

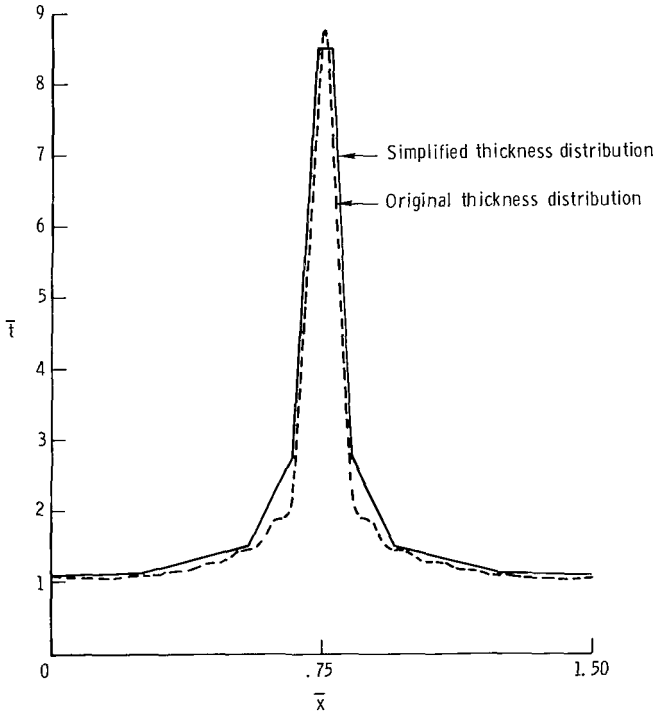

Figure 17.- Original and simplified thickness distributions. p = 1000 psi (6.9 MN/m^2); $\bar{x}_1$ = 1.5; $\bar{y}_o$ = 0; ω = 0.2.

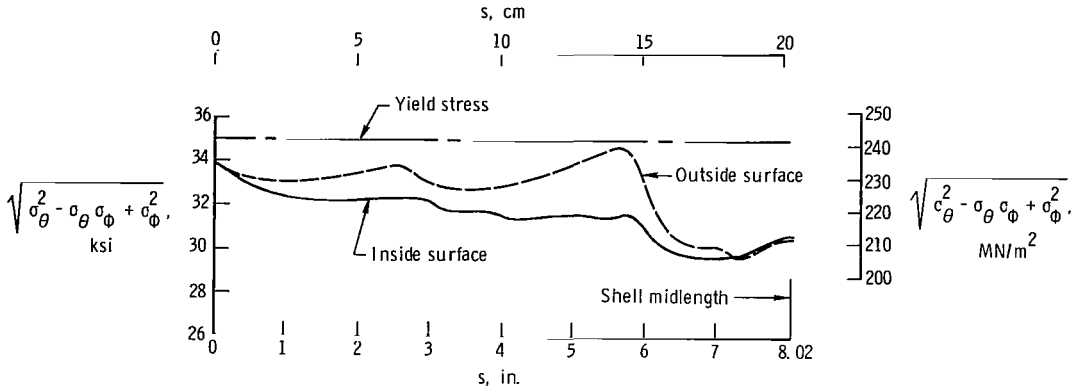

Figure 18.- The stress quantity $\sqrt{\sigma_\theta^2 - \sigma_\theta\sigma_\phi + \sigma_\phi^2}$ at the inner and outer surfaces of a transition section with simplified thickness distribution as a function of distances from left end measured along the meridian. p = 1000 psi (6.9 MN/m^2); y_o = 10 in. (25.4 cm); x_1 = 15 in. (38.1 cm); y_o' = 0; ω = 0.2.

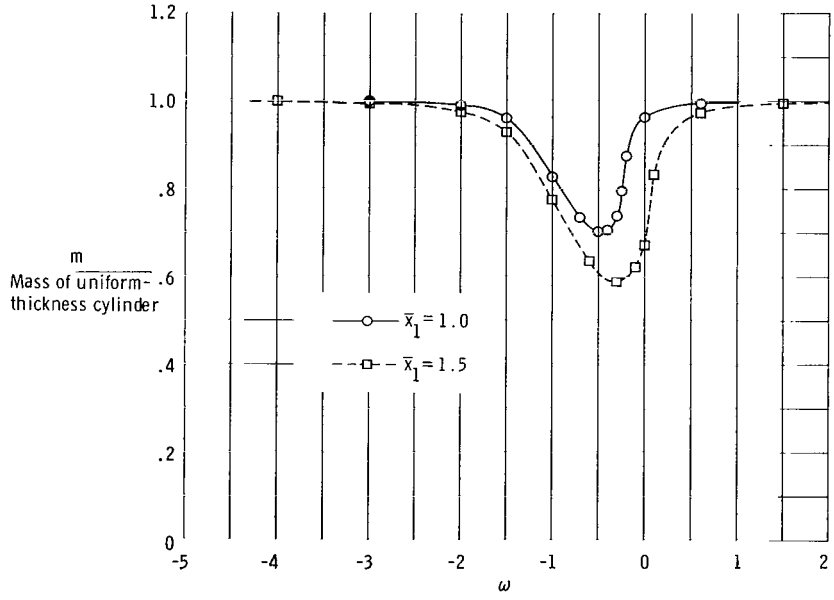

Figure 19.- Ratio of mass m of minimum-mass transition section to mass of uniform-thickness cylinders designed to support same load, as a function of loading parameter ω. Transition sections have zero-slope end conditions.

The radius of the cylinders is y_o, the radius of the transition sections at the ends. The length of the cylinders is the same as the length of the corresponding transition section. The upper curve is for $\bar{x}_1 = 1.0$ and the lower curve is for $\bar{x}_1 = 1.5$. The Von Mises yield condition is the critical stress condition for the cylinders as well as the transition sections. The symbols indicate calculated designs. The maximum mass saving for the shorter transition sections, $\bar{x}_1 = 1.0$, is about 29 percent. The maximum mass saving for the longer transition sections, $\bar{x}_1 = 1.5$, is about 41 percent. For large positive or negative values of ω the axial load F_o is the dominant load, and the minimum-mass transition section which is symmetric about the midlength and has zero-slope end conditions approaches a cylinder.

Pressure-Vessel Heads

Equation (33) was used to derive the minimum-mass shapes and thickness distributions for three pressure-vessel heads. The design parameter that differentiates among these three heads is the slope of the head at its junction with the pressure vessel. One of the heads is designed for use with a cylindrical pressure vessel, and in this case the

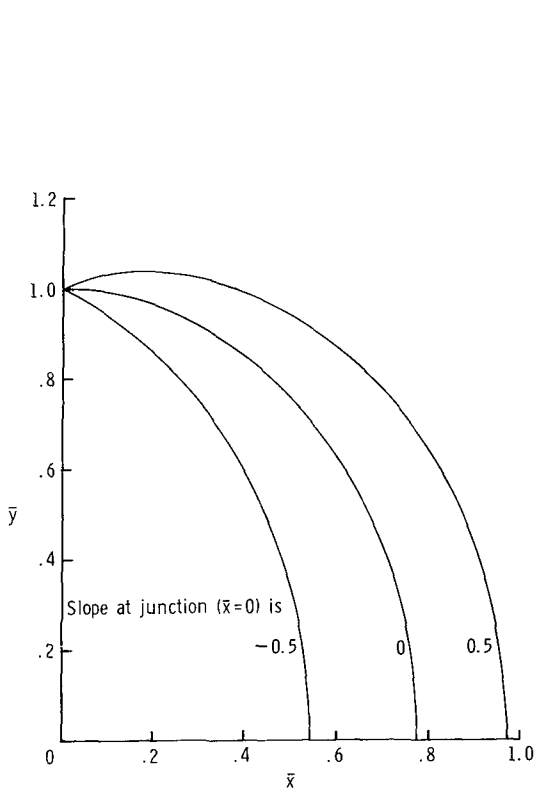

(a) Nondimensional meridional shape.

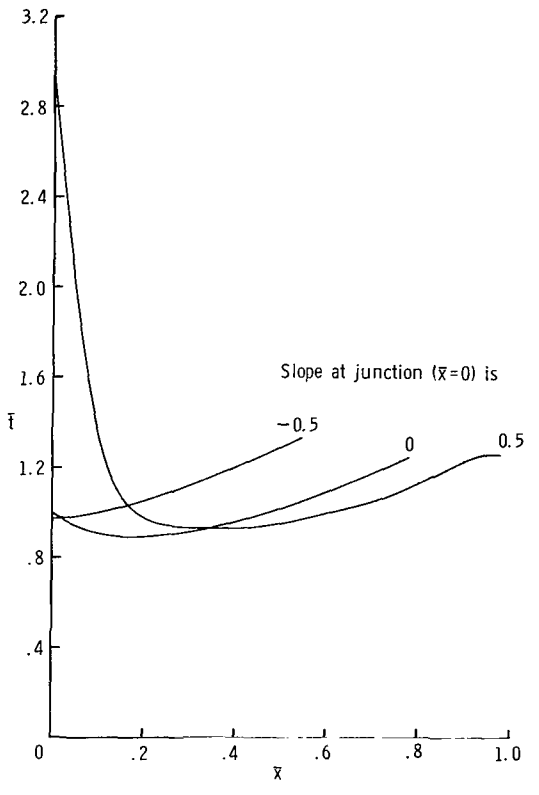

(b) Nondimensional thickness distribution.

Figure 20.- Nondimensional meridional shapes, thickness distributions, and stress resultants for minimum-mass pressure-vessel heads with slopes at the head-vessel junction equal to -0.5, 0, and 0.5.

slope of the head at the junction is zero. Each of the other two heads has a nonzero-slope end condition and can therefore be used with conical or ellipsoidal pressure vessels. One of these heads has a slope equal to 0.5 at the junction, and the other has a slope equal to -0.5.

Shapes.- The shapes for the three pressure-vessel heads are shown in figure 20(a). As in the case of the transition sections, the X-axis is the axis of revolution. The nondimensional head depths are 0.54, 0.77, and 0.97 for minimum-mass heads having slopes at the junction of -0.5, 0, and 0.5, respectively. For these junction slopes, the minimum-mass heads obtained by using the series given in equation (33) are 0.01, 0.4, and 5.4 percent lighter, respectively, than heads obtained by using the best ellipse.

Thickness distributions.- The thickness $\bar{t}$ for each of the three heads is shown as a function of the axial coordinate $\bar{x}$ in figure 20(b) and as a function of the distance $\bar{s}$ measured along the meridian in figure 20(c). Note that $d\bar{t}/d\bar{s} = 0$ at the apex.

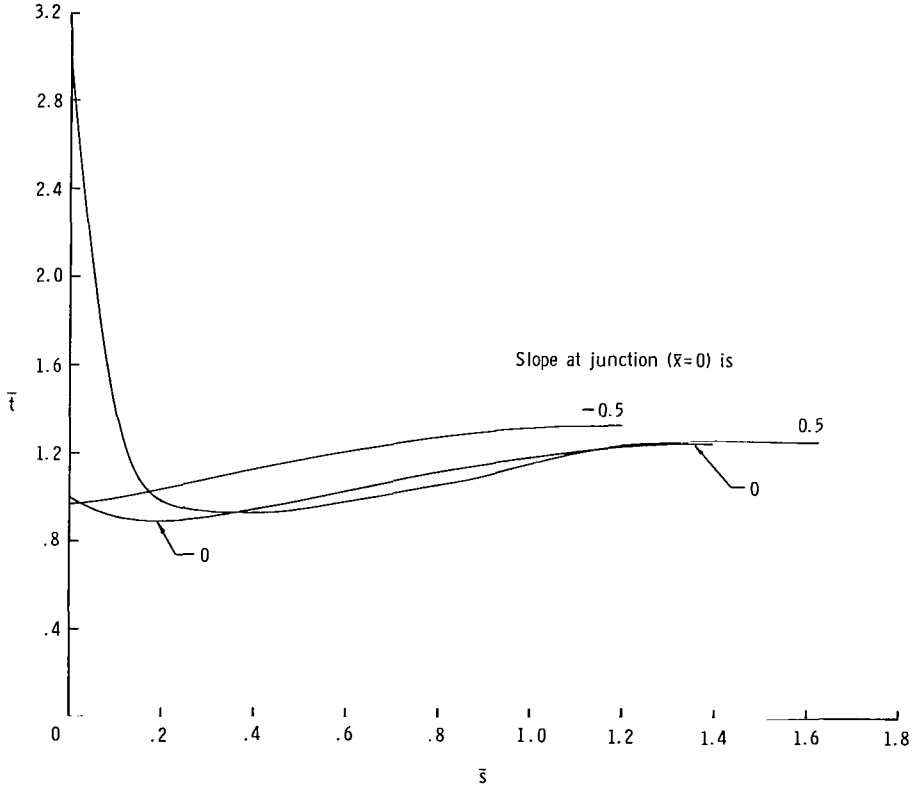

(c) Nondimensional thickness $\bar{t}$ as a function of nondimensional distance $\bar{s}$ along the meridian.

Figure 20.- Continued.

According to the theory considered in this report, a discontinuity in thickness can exist between the head and the pressure vessel at their junction. Consider the head which has a zero-slope end condition and a cylindrical shell to which the head could be attached. If the cylinder is loaded only by pressure and if the thickness of the cylinder, like the thickness of the head, is determined by the Von Mises yield condition, then the thickness of the head at the junction is about six-tenths the thickness of the cylinder.

Stress resultants.- Both the circumferential and meridional stress resultants for the three heads are shown as functions of the axial coordinate $\bar{x}$ in figure 20(d). For each head the circumferential stress resultant $\bar{N}_\theta$ is shown as a solid line and the meridional stress resultant $\bar{N}_\phi$ is shown as a dashed line. In each case the stress resultants are equal, as they should be, at the apex. For the head having an end slope of 0.5 a large compressive circumferential stress occurs near its junction with the pressure

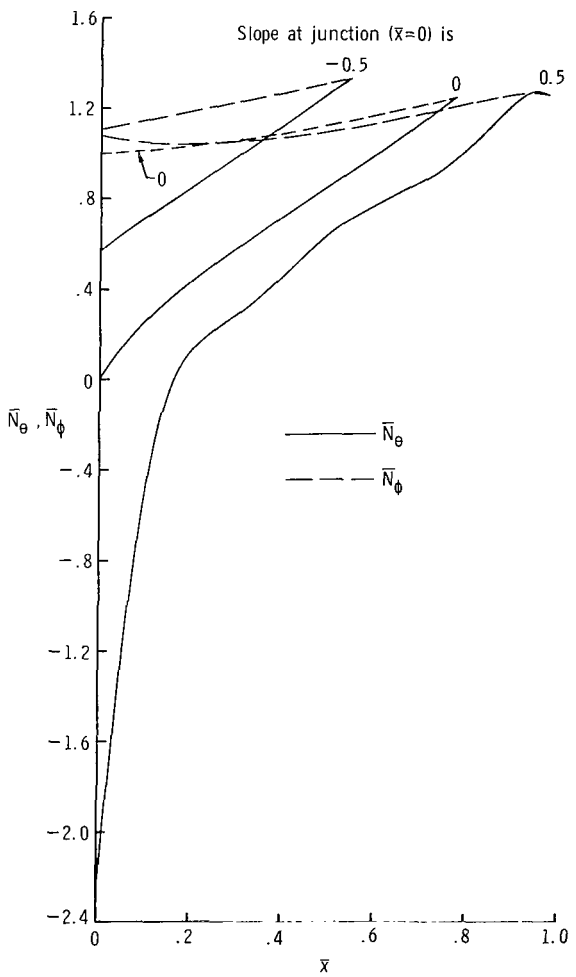

(d) Nondimensional stress distributions.

Figure 20.- Concluded.

vessel. Compressive stresses are discussed in a previous section entitled "Negative (compressive) stresses, buckling, and constraints."

The masses and Ritz coefficients for each of these heads are given in table V.

Discontinuity bending stresses.- If the slopes of the head and the pressure vessel are equal at the junction, then the meridional stress resultant is continuous across the junction. But, within the framework of linear membrane shell theory, a discontinuity in the circumferential stress resultant will occur if there is a discontinuity in curvature at the junction. For the theory considered herein, it is not possible to generate minimum-mass pressure-vessel heads so that curvatures match at the junction. The permissible boundary conditions are limited to coordinates and slopes.

In an actual loaded pressure vessel which has a discontinuity in curvature at the head-vessel junction, bending occurs at the junction, allowing the stresses and deflections to be continuous across the junction. If both the pressure vessel and the head are thin, if they are tangent at the junction, and if the discontinuity in curvature is not large, the discontinuity bending stresses will be local and the head can be designed on the basis of membrane theory together with local reinforcement at the junction. For example, according to reference 13, the mass of the reinforcement needed for an ellipsoidal head to be used with a cylindrical tank amounts to slightly more than 1 percent of the head mass.

Minimum-mass pressure-vessel heads that are to be used with cylindrical pressure vessels are also considered in reference 13. As in the present report, linear membrane theory and the Von Mises yield condition are used in reference 13 for design purposes. The limitation to coordinate and slope boundary conditions is therefore applicable to the work in reference 13. Unlike the present report, which considers unconstrained shapes, reference 13 investigates three constrained classes of pressure-vessel heads – ellipsoidal, torispherical, and Cassinian oval – and minimizes the mass with respect to a single shape parameter for each class of shells. In reference 13 the ellipsoidal head is found to be the lightest of the three types of heads considered. The present analysis leads to the conclusion that for cylindrical pressure vessels (junction slope equal to zero), the ellipsoidal head is essentially the lightest head of all possible shapes.

Cassinian-type pressure-vessel heads are considered in reference 13 because they provide zero curvature at the cylinder-head junction and thereby minimize discontinuity bending stresses. Two important comments should be made with regard to Cassinian heads and minimum-mass pressure-vessel heads. First, within the framework of linear membrane theory it is not appropriate to derive minimum-mass pressure-vessel heads of the Cassinian type because prescription of curvature boundary conditions is not allowed. And, second, since Cassinian heads include only a small portion of the head shapes that have a zero-curvature boundary condition, conclusions based on Cassinian

heads cannot be extended to all heads that have zero-curvature boundary conditions or to other head shapes that are tailored to minimize discontinuity bending stresses.

To demonstrate both these comments, equation (33) was used to generate a pressure-vessel head with the following boundary conditions at the junction of the head and vessel:

$$\bar{y}(0) = 1 \tag{37}$$

$$\bar{y}'(0) = 0 \tag{38}$$

$$\bar{y}''(0) = 0 \tag{39}$$

Ten terms were used to define the shape. It is of interest to compare this pressure-vessel head with the minimum-mass head that has only equations (37) and (38) as boundary conditions. The shapes are almost identical. The zero-curvature head weighs about 3 percent more than the head without this additional constraint. (The lightest Cassinian head weighs almost 50 percent more than the minimum-mass head without the additional zero-curvature restraint.) The nondimensional circumferential stress resultants for both heads are shown in figure 21. The solid curve is for the head that has zero curvature and slope at the junction. The dashed curve is for the minimum-mass head with only the zero-slope boundary condition. Both these curves are based on linear membrane theory. For the zero-curvature head, $\bar{N}_\theta$ is constrained to be 2.0 at the junction $\bar{x} = 0$. The stress then falls off rapidly and oscillates about the dashed curve. As more

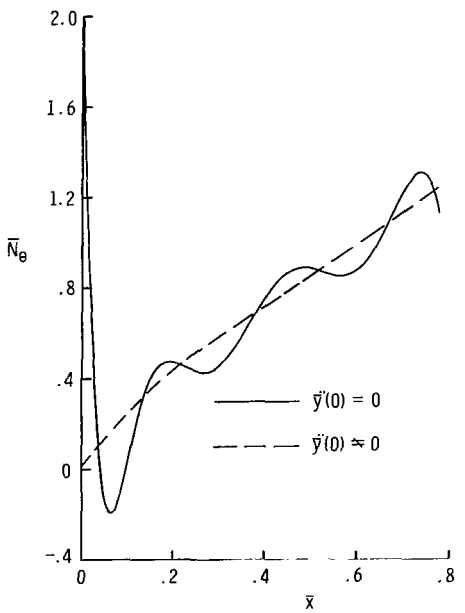

Figure 21.- Nondimensional circumferential stress resultants for pressure-vessel head with boundary conditions $\bar{y}(0) = 1$, $\bar{y}'(0) = 0$, $\bar{y}''(0) = 0$ and for minimum-mass head with boundary conditions $\bar{y}(0) = 1$, $\bar{y}'(0) = 0$.

terms are added to the series, the stress distributions for the two heads will almost coincide except near $\bar{x} = 0$. In effect, the solution is trying to ignore the improper curvature boundary condition.

CONCLUDING REMARKS

A method has been presented for calculating the shape and thickness distribution of a minimum-mass shell of revolution for given coordinate and slope end conditions and given values of axial load and pressure load. Linear membrane shell theory was used to relate the loading and shape to the stress resultants, and the strain energy of distortion (Von Mises) yield condition was used to relate the stress resultants to the thickness. Membrane theory greatly simplifies the calculations and appears to be sufficiently accurate for the type of shell problems considered. Moreover, the results obtained by using membrane theory could serve as the first approximation for calculations based on more sophisticated shell theories.

Two types of shell shapes are considered: transition sections, which are open at both ends, and pressure-vessel heads, which are open at one end and closed at the other. The results show that minimum-mass transition sections have a tendency to neck down away from the ends. They may have large excursions in the thickness distribution. Examples which make use of inequality constraints on the stress resultants are included. Inequality constraints can also be imposed on the shape and thickness distribution to restrain both the necking down of the shape and the large excursions in the thickness distributions. When comparisons are made between minimum-mass transition sections and constant-thickness cylinders having the same length and radius and designed to carry the same load, the minimum-mass transition sections are, for some loadings, 30 to 40 percent lighter than the corresponding cylinder. The calculations for pressure-vessel heads are applicable for use with conical and ellipsoidal as well as cylindrical pressure vessels.

Langley Research Center,
National Aeronautics and Space Administration,
Hampton, Va., October 26, 1970.

APPENDIX

CONVERSION OF U.S. CUSTOMARY UNITS TO SI UNITS

Conversion factors (ref. 15) for the units used in this report are given in the following table:

Physical quantity	U.S. Customary Unit	Conversion factor (*)	SI Unit (**)
Length	in.	0.0254	meters (m)
Stress Modulus of elasticity	ksi	6.895×10^6	newtons/meter^2 (N/m^2)
Pressure	psi	6.895×10^3	newtons/meter^2 (N/m^2)

*Multiply value given in U.S. Customary Units by conversion factor to obtain equivalent value in SI Units.

**Prefixes to indicate multiples of units are as follows:

Prefix	Multiple
giga (G)	10^9
mega (M)	10^6

REFERENCES

1. Freiberger, Walter: Minimum Weight Design of Cylindrical Shells. J. Appl. Mech., vol. 23, no. 4, Dec. 1956, pp. 576-580.

2. Drucker, D. C.; and Shield, R. T.: Design for Minimum Weight. IX^{e} Congrès International de Mêcanique Appliquée, Tome V, Univ. of Brussels, 1957, pp. 212-222.

3. Drucker, D. C.; and Shield, R. T.: Bounds on Minimum Weight Design. Quart. Appl. Math., vol. XV, no. 3, Oct. 1957, pp. 269-281.

4. Freiberger, Walter F.: On the Minimum Weight Design Problem for Cylindrical Sandwich Shells. J. Aeronaut. Sci., vol. 24, no. 11, Nov. 1957, pp. 847-848.

5. Mróz, Zenon: On a Problem of Minimum Weight Design. Tech. Rep. No. 59 (Contract Nonr 562(10)), Div. Appl. Math., Brown Univ., May 1960.

6. Shield, R. T.: On the Optimum Design of Shells. Trans. ASME, Ser. E: J. Appl. Mech., vol. 27, no. 2, June 1960, pp. 316-322.

7. Shield, Richard Thorpe: Optimum Design Methods for Multiple Loading. Z. Angew. Math. Phys., vol. 14, no. 1, 1963, pp. 38-45.

8. Shamiyev, F. G.: Designing Minimum-Weight Shells. FTD-TT-64-953, U.S. Air Force, Feb. 8, 1965. (Available from DDC as AD 611533.)

9. Sheu, C. Y.; and Prager, W.: Optimal Plastic Design of Circular and Annular Sandwich Plates With Piecewise Constant Cross Section. Tech. Rep. No. 18 (Contract N00014-67-A-0109-0003), Dep. Aerosp. Mech. Eng. Sci., Univ. of California, San Diego, June 1968.

10. Wang, Han-Chung; and Worley, Will J.: An Approach to Optimum Shape Determination for a Class of Thin Shells of Revolution. Trans. ASME, Ser. E: J. Appl. Mech., vol. 35, no. 3, Sept. 1968, pp. 524-529.

11. Keith, Harold Dean: Minimum Weight Design of Axially Symmetric Shells of Revolution. Ph.D. Thesis, Univ. of Illinois, 1967.

12. Hoffman, G. A.: Minimum-Weight Proportions of Pressure-Vessel Heads. Trans. ASME, Ser. E: J. Appl. Mech., vol. 29, no. 4, Dec. 1962, pp. 662-668.

13. Hoffman, George A.: Optimal Proportions of Pressure Vessel Heads. J. Aerosp. Sci., vol. 29, no. 12, Dec. 1962, pp. 1471-1475.

14. Bert, C. W.: Ellipsoidal Closures for Minimum-Weight Pressure Vessels. Can. Aeronaut. Space J., vol. 9, no. 5, May 1963, pp. 133-136.

15. Comm. on Metric Pract.: ASTM Metric Practice Guide. NBS Handbook 102, U.S. Dep. Com., Mar. 10, 1967.

16. Scarborough, James B.: Numerical Mathematical Analysis. Fifth ed., Johns Hopkins Press, 1962, pp. 213-221.

17. Fletcher, R.; and Powell, M. J. D.: A Rapidly Convergent Descent Method for Minimization. Computer J., vol. 6, no. 2, July 1963, pp. 163-168.

18. Thornton, William A.; and Schmit, Lucien A., Jr.: The Structural Synthesis of an Ablating Thermostructural Panel. NASA CR-1215, 1968.

19. Morrow, William M., II; and Schmit, Lucien A., Jr.: Structural Synthesis of a Stiffened Cylinder. NASA CR-1217, 1968.

20. Schmit, L. A., Jr.; Morrow, W. M., II; and Kicher, T. P.: A Structural Synthesis Capability for Integrally Stiffened Cylindrical Shells. AIAA Pap. No. 68-327, Apr. 1968.

21. Fiacco, Anthony V.; and McCormick, Garth P.: Nonlinear Programming: Sequential Unconstrained Minimization Techniques. John Wiley & Sons, Inc., c.1968.

22. Bracken, Jerome; and McCormick, Garth P.: Selected Applications of Nonlinear Programming. John Wiley & Sons, Inc., c.1968.

23. Sepetoski, W. K.; Pearson, C. E.; Dingwell, I. W.; and Adkins, A. W.: A Digital Computer Program for the General Axially Symmetric Thin-Shell Problem. Trans. ASME, Ser. E: J. Appl. Mech., vol. 29, no. 4, Dec. 1962, pp. 655-661.

TABLE I.- RITZ COEFFICIENTS c_n FOR SEVERAL TYPICAL MINIMUM-MASS TRANSITION SECTIONS

(a) Zero-slope end conditions; $\bar{x}_1 = 1.0$

n	c_n for –		
	$\omega = -0.4$ $\overline{m} = 1.258$	$\omega = 0$ $\overline{m} = 1.668$	$\omega = 0.6$ $\overline{m} = 1.823$
1	-3.961×10^{-1}	-7.570×10^{-2}	-1.095×10^{-2}
2	1.319×10^{-1}	9.143×10^{-3}	-3.512×10^{-4}
3	-4.686×10^{-2}	-2.784×10^{-3}	-8.159×10^{-5}
4	7.312×10^{-3}	9.501×10^{-4}	-2.558×10^{-5}
5	9.784×10^{-3}	-4.453×10^{-4}	-1.054×10^{-5}
6	-1.427×10^{-2}	1.973×10^{-4}	-5.948×10^{-6}
7	1.190×10^{-2}	-1.086×10^{-4}	
8	-6.863×10^{-3}	5.251×10^{-5}	
9	1.891×10^{-3}	-3.079×10^{-5}	
10	1.534×10^{-3}	1.388×10^{-5}	
11	-3.039×10^{-3}	-7.670×10^{-6}	
12	2.960×10^{-3}	1.519×10^{-6}	
13	-1.989×10^{-3}		
14	8.069×10^{-4}		
15	1.132×10^{-4}		
16	-5.837×10^{-4}		
17	6.471×10^{-4}		
18	-4.732×10^{-4}		
19	2.416×10^{-4}		
20	-7.182×10^{-5}		

TABLE I.- RITZ COEFFICIENTS c_n FOR SEVERAL TYPICAL MINIMUM-MASS TRANSITION SECTIONS – Continued

(b) Zero-slope end conditions; $\bar{x}_1 = 1.5$

n	c_n for –		
	$\omega = 0$ $\overline{m} = 1.747$	$\omega = 0.2$ $\overline{m} = 2.353$	$\omega = 0.6$ $\overline{m} = 2.674$
1	-6.670×10^{-1}	-2.345×10^{-1}	-6.012×10^{-2}
2	2.587×10^{-1}	4.199×10^{-2}	6.636×10^{-4}
3	-1.508×10^{-1}	-1.594×10^{-2}	-4.597×10^{-4}
4	9.830×10^{-2}	7.199×10^{-3}	-6.442×10^{-5}
5	-6.946×10^{-2}	-4.046×10^{-3}	-4.103×10^{-5}
6	5.047×10^{-2}	2.355×10^{-3}	-1.777×10^{-5}
7	-3.761×10^{-2}	-1.515×10^{-3}	-9.176×10^{-6}
8	2.814×10^{-2}	9.679×10^{-4}	-8.043×10^{-6}
9	-2.118×10^{-2}	-6.537×10^{-4}	
10	1.582×10^{-2}	4.284×10^{-4}	
11	-1.174×10^{-2}	-2.881×10^{-4}	
12	8.571×10^{-3}	1.824×10^{-4}	
13	-6.148×10^{-3}	-1.142×10^{-4}	
14	4.286×10^{-3}	6.103×10^{-5}	
15	-2.893×10^{-3}	-2.628×10^{-5}	
16	1.857×10^{-3}		
17	-1.117×10^{-3}		
18	6.060×10^{-4}		
19	-2.766×10^{-4}		
20	8.700×10^{-5}		

TABLE I.- RITZ COEFFICIENTS c_n FOR SEVERAL TYPICAL MINIMUM-MASS TRANSITION SECTIONS – Concluded

(c) End conditions: $\bar{y}'_0 = 0.5$; $\bar{x}_1 = 1.5$

n	c_n for –		
	$\omega = -0.4$ $\overline{m} = 1.718$	$\omega = 0$ $\overline{m} = 2.294$	$\omega = 0.6$ $\overline{m} = 2.605$
1	-5.936×10^{-1}	-8.310×10^{-2}	-2.800×10^{-2}
2	1.696×10^{-1}	-1.850×10^{-3}	-2.491×10^{-3}
3	-6.654×10^{-2}	-1.350×10^{-3}	-5.757×10^{-4}
4	9.176×10^{-3}	-3.190×10^{-4}	-1.965×10^{-4}
5	1.271×10^{-2}	-1.661×10^{-4}	-8.378×10^{-5}
6	-1.959×10^{-2}	-7.702×10^{-5}	-4.116×10^{-5}
7	1.595×10^{-2}	-4.362×10^{-5}	-2.222×10^{-5}
8	-9.262×10^{-3}	-2.571×10^{-5}	-1.272×10^{-5}
9	2.277×10^{-3}	-1.595×10^{-5}	-7.473×10^{-6}
10	2.321×10^{-3}	-1.098×10^{-5}	
11	-4.411×10^{-3}	-6.224×10^{-6}	
12	4.183×10^{-3}	-6.929×10^{-6}	
13	-2.795×10^{-3}		
14	1.065×10^{-3}		
15	2.350×10^{-4}		
16	-9.189×10^{-4}		
17	9.861×10^{-4}		
18	-7.314×10^{-4}		
19	3.739×10^{-4}		
20	-1.227×10^{-4}		

TABLE II.- RITZ COEFFICIENTS c_n FOR MINIMUM-MASS TRANSITION SECTION WITH PRESSURE $p = 0$, $\bar{y}_o' = 0.5$, AND $\bar{x}_1 = 1.5$

$$\left[\frac{m\sigma_c}{2\pi y_o^2 \rho F_o} = 2.309\right]$$

n	c_n
1	-7.731×10^{-2}
2	-1.282×10^{-2}
3	-4.310×10^{-3}
4	-1.943×10^{-3}
5	-1.029×10^{-3}
6	-6.025×10^{-4}
7	-3.777×10^{-4}
8	-2.483×10^{-4}
9	-1.688×10^{-4}
10	-1.174×10^{-4}
11	-8.283×10^{-5}
12	-5.870×10^{-5}
13	-4.134×10^{-5}
14	-2.844×10^{-5}
15	-1.850×10^{-5}
16	-1.030×10^{-5}

TABLE III.- RITZ COEFFICIENTS c_n FOR MINIMUM-MASS TRANSITION SECTION WITH $\omega = -1.0$ AND $\bar{x}_1 = 1.5$

$$\begin{bmatrix} \overline{m} = 2.328 \\ \bar{y}_o' = -2.784 \end{bmatrix}$$

n	c_n
1	6.433×10^{-1}
2	1.367×10^{-1}
3	5.313×10^{-2}
4	2.641×10^{-2}
5	1.499×10^{-2}
6	9.216×10^{-3}
7	5.970×10^{-3}
8	3.998×10^{-3}
9	2.730×10^{-3}
10	1.879×10^{-3}
11	1.288×10^{-3}
12	8.654×10^{-4}
13	5.561×10^{-4}
14	3.255×10^{-4}
15	1.931×10^{-4}
16	1.103×10^{-4}
17	5.488×10^{-5}

TABLE IV.- RITZ COEFFICIENTS c_n FOR MINIMUM-MASS TRANSITION SECTIONS WITH STRESS RESULTANT CONSTRAINT

$[\omega = -0.4$; zero-slope conditions; $\bar{x}_1 = 1.0]$

(a) Design for $\overline{N}_\theta < 2.5$; $\overline{m} = 1.565$

n	c_n
1	-1.435×10^{-1}
2	-6.200×10^{-3}
3	1.974×10^{-3}
4	1.422×10^{-3}
5	4.565×10^{-5}
6	-3.718×10^{-4}
7	-1.734×10^{-4}
8	5.400×10^{-5}
9	9.245×10^{-5}
10	1.282×10^{-5}
11	-3.666×10^{-5}
12	-2.532×10^{-5}
13	6.120×10^{-7}
14	1.075×10^{-5}
15	5.876×10^{-6}

(b) Design for no negative stresses; $\overline{m} = 1.277$

n	c_n
1	-3.478×10^{-1}
2	1.030×10^{-1}
3	-3.058×10^{-2}
4	-7.938×10^{-4}
5	1.350×10^{-2}
6	-1.650×10^{-2}
7	1.443×10^{-2}
8	-1.039×10^{-2}
9	6.251×10^{-3}
10	-3.011×10^{-3}
11	9.632×10^{-4}
12	2.698×10^{-5}
13	-3.068×10^{-4}
14	2.351×10^{-4}
15	-8.651×10^{-5}

TABLE V.- NONDIMENSIONAL MASS $\overline{m}$ AND RITZ COEFFICIENTS c_n FOR MINIMUM-MASS PRESSURE-VESSEL HEADS WITH SLOPE AT HEAD-VESSEL JUNCTION EQUAL TO -0.5, 0, AND 0.5

n	c_n for –		
	Slope = -0.5 $\overline{m}$ = 0.7412 $\bar{b}$ = 0.5433	Slope = 0 $\overline{m}$ = 0.8503 $\bar{b}$ = 0.7739	Slope = 0.5 $\overline{m}$ = 1.249 $\bar{b}$ = 0.9749
0	1.203	1.387	1.564
1	-1.828×10^{-1}	-3.350×10^{-1}	-2.334×10^{-1}
2	-1.783×10^{-2}	2.038×10^{-2}	-8.173×10^{-1}
3	1.429×10^{-3}	-1.448×10^{-1}	7.024×10^{-1}
4	-3.483×10^{-3}	1.311×10^{-1}	1.111
5	-5.433×10^{-5}	-5.914×10^{-2}	-2.414
6			1.520×10^{-1}
7			1.894
8			-8.596×10^{-1}
9			-9.918×10^{-2}

"The aeronautical and space activities of the United States shall be conducted so as to contribute . . . to the expansion of human knowledge of phenomena in the atmosphere and space. The Administration shall provide for the widest practicable and appropriate dissemination of information concerning its activities and the results thereof."

—NATIONAL AERONAUTICS AND SPACE ACT OF 1958

NASA SCIENTIFIC AND TECHNICAL PUBLICATIONS

TECHNICAL REPORTS: Scientific and technical information considered important, complete, and a lasting contribution to existing knowledge.

TECHNICAL NOTES: Information less broad in scope but nevertheless of importance as a contribution to existing knowledge.

TECHNICAL MEMORANDUMS: Information receiving limited distribution because of preliminary data, security classification, or other reasons.

CONTRACTOR REPORTS: Scientific and technical information generated under a NASA contract or grant and considered an important contribution to existing knowledge.

TECHNICAL TRANSLATIONS: Information published in a foreign language considered to merit NASA distribution in English.

SPECIAL PUBLICATIONS: Information derived from or of value to NASA activities. Publications include conference proceedings, monographs, data compilations, handbooks, sourcebooks, and special bibliographies.

TECHNOLOGY UTILIZATION PUBLICATIONS: Information on technology used by NASA that may be of particular interest in commercial and other non-aerospace applications. Publications include Tech Briefs, Technology Utilization Reports and Technology Surveys.

Details on the availability of these publications may be obtained from:

SCIENTIFIC AND TECHNICAL INFORMATION OFFICE

NATIONAL AERONAUTICS AND SPACE ADMINISTRATION

Washington, D.C. 20546